LIGHTHOUSE

SWEDISH MARITIME COMPETENCE CENTRE

LIGHTHOUSE REPORTS

ELÄTTRA

Utilization of high-strength steel for weight reduction of large electric ships

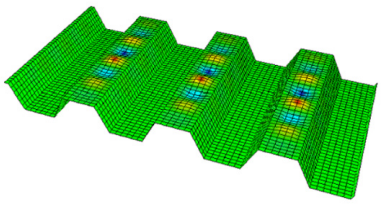

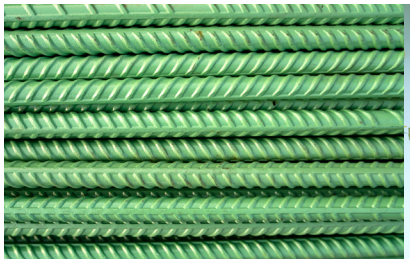

An innovation project made within the Swedish Transport Administration's industry program Sustainable Shipping, operated by Lighthouse, published in November 2024

www.lighthouse.nu

ELÄTTRA

Utilization of high-strength steel for weight reduction of large electric ships

Authors

Ramin Moshfegh & Andreas Bach, RISE Research Institutes of Sweden

Zhiyuan Li & Jonas W Ringsberg, Chalmers University of Technology

David Gotvall, MacGregor AB

In association with

Stena Rederi AB and SSAB

An innovation project run within the Swedish Transport Administration's industry program Sustainable Shipping, operated by Lighthouse

Summary

This document is the final report for the innovation project ELÄTTRA, which is part of Trafikverket's industry program "Hållbar Sjöfart". This program is run by Lighthouse and the project has been conducted by RISE Research Institutes of Sweden and Chalmers University of Technology in cooperation with the industrial partners Stena Rederi AB, MacGregor AB, and SSAB.

The ELÄTTRA project is a follow-up project of the Lighthouse project Electric Light, in which an electric driven RoPax was conceptualized and designed. The Electric Light project concluded that it is crucial to construct electric ships with lightweight and fire-safe materials, which implies that extra high-strength steels are more suitable than aluminum and composite materials for this type of ship structure. Currently, extra high-strength steels are only recommended for building highly specialized applications onboard ships according to class rules. The ELÄTTRA project investigated the potential of re-designing ship structures and sub-structures using extra high-strength steels. The main goal is to develop a practical engineering approach for structural design/optimization of deck structures and the effects on weight reduction. Deck structures of Ro-Ro ships have been selected as the representative structural components to demonstrate the proposed methodology.

The project has carried out the following activities:

- Evaluation of the buckling capacities as well as the weight-reduction potential of the re-design using extra high-strength steels.
- Optimization with respect to weight, taking the increased tensile strength, buckling, and deflection as constraints.
- Estimation of fatigue life reduction when introducing extra high-strength steels.
- Non-linear buckling behaviors with initial imperfection.

The results from this project show that the proposed methodology is a suitable tool for structural re-design and optimization when introducing extra high-strength steel. In addition, in this work, we selected a Stena RoPax and carried out strength analyses of the car-deck and the stern-ramp. For the car-deck, linear buckling and non-linear analyses were conducted and compared. For the stern-ramp, we focused on the strength check of the limits of the deflection that is specified by the class rules. These analyses again highlighted the great weight-reduction potential of introducing extra high-strength steels in Ro-Pax vessels.

Sammanfattning

Detta dokument är slutrapporten för innovationsprojektet ELÄTTRA, som är en del av Trafikverkets branschprogram "Hållbar Sjöfart". Programmet drivs av Lighthouse och projektet har genomförts av RISE Research Institutes of Sweden och Chalmers tekniska högskola i samarbete med industripartnerna Stena Rederi AB, MacGregor AB och SSAB.

ELÄTTRA-projektet är ett uppföljningsprojekt av Lighthouseprojektet Lätta elfartyg/ Electric Light, där en eldriven RoPax-färja konceptualiserades och designades. Electric Light-projektet konstaterade att det är avgörande att bygga elektriska fartyg med lätta och brandsäkra material, vilket innebär att extra höghållfasta stål är mer lämpade än aluminium och kompositmaterial för denna typ av fartygsstruktur. För närvarande rekommenderas extra höghållfasta stål endast för att bygga högt specialiserade applikationer ombord på fartyg enligt klassreglerna. ELÄTTRA-projektet undersökte potentialen för att omdesigna fartygsstrukturer och delstrukturer med hjälp av extra höghållfasta stål. Huvudmålet är att utveckla ett praktiskt ingenjörsmässigt tillvägagångssätt för strukturell design/optimering av däckstrukturer och effekterna på viktminskning. Däckstrukturer för Ro-Ro-fartyg har valts som representativa strukturella komponenter för att demonstrera den föreslagna metoden.

Projektet har genomfört följande aktiviteter:

- Utvärdering av bucklingskapaciteten samt viktminskningspotentialen vid omdesign med extra höghållfasta stål.
- Optimering avseende vikt, med hänsyn till den ökade draghållfastheten, buckling och deformation som begränsningar.
- Beräkning av minskad utmattningslivslängd vid introduktion av extra höghållfasta stål.
- Undersökning av icke-linjära bucklingsbeteenden med initiala imperfektioner.

Projektet har visat att den föreslagna metoden är ett lämpligt verktyg för strukturell omdesign och optimering vid introduktion av extra höghållfast stål. Dessutom valde vi i detta arbete en Stena RoPax och genomförde hållfasthetsanalyser av bildäck och akterramp. För bildäcket genomfördes linjära bucklingsanalyser och icke-linjära analyser, som jämfördes. För akterrampen fokuserade vi på hållfasthetskontrollen av gränserna för deformationen som specificeras i klassreglerna. Dessa analyser betonade återigen den stora viktminskningspotentialen vid introduktion av extra höghållfasta stål i RoPax-fartyg.

Abbreviations

BISO	Bilinear Isotropic Hardening
CS	Classification Society
EHSS	Extra High Strength Steel
FEA	Finite Element Analysis
FEM	Finite Element Method
GHG	Green House Gases
HSS	High Strength Steel
IMO	International Maritime Organization
Ro-Pax	Roll on Roll off cargo ship with Passengers
Ro-Ro	Roll on Roll off cargo ship
UDL	Uniformly Distributed Loads

Contents

List of Tables

List of Figures

1 Introduction

The European Commission and International Maritime Organization (IMO) have launched legislation aimed at reducing EU GHG emissions by 55% by 2030 [1] and 40% of international shipping's carbon intensity by the same year. This could help reduce global CO2 emissions from ships, estimated at around 0.9 Gt per year [2]. Energy efficiency in shipping is crucial for economic reasons, promoting alternative fuels, materials, and changes in ship design and construction. The Lighthouse innovation project Electric Light suggests using extra high-strength steel to reduce design weight [3] and enable emission-free, light, electrically powered transportation in Swedish and international waterways. The use of high-strength steel for general and detail construction occurs at a TRL level between 6-7, serving as a demonstration basis for rule change proposals. The project concept aims to enhance Swedish collaboration and competence in the steel sector, with a vision of a large, zero-emission ferry. Stena Elektra plans to design and manufacture an electric ship for a 2030 launch. The project aims to reduce functional weight while maintaining the intended purpose of items, a key focus in enhancing fuel economy.

This study is aimed to reduce ship weight by employing high-strength steel that is almost twice as strong as ordinary HT36 steel [4]. The objective is to minimize the thickness of specific components, such as the vehicle/car deck, which covers a large amount of a RoPax vessel while preserving component rigidity. The fact that lighter ships need less energy to move across water means that a 10–20% weight decrease can save 5–10% on fuel in comparison with e.g. a reduction in hull resistance can save up to 3% of fuel usage or a reduction in propulsion power can save up to 2%.

Main Theme: This study investigates the potential for weight reduction in ship structures by utilizing high-strength steel. The research focuses on developing a methodology for assessing this potential, specifically for typical ship structures composed of stiffened panels.

Key Ideas & Facts:

Sustainability and Environmental Impact: The project is driven by the need for sustainable shipping practices. Utilizing high-strength steel can significantly reduce material consumption and ship weight, leading to lower energy consumption and a reduced environmental footprint. The study emphasizes the future possibility of recycling steel using renewable energy.

Methodology Focus: The research concentrates on developing a methodology for evaluating the weight reduction potential when incorporating higher tensile strength steels. The methodology is specifically targeted towards ship structures with stiffened panels.

Finite Element Analysis (FEA) Scope: FEA simulations were employed, focusing on static and buckling analyses. While details like slots and lugs were included in the models, welding details were excluded. The study acknowledges the limitations of not considering welding procedures' effects on material properties.

Buckling Analysis: Both linear and non-linear buckling phenomena were investigated. Although initial imperfections were considered in the non-linear analysis, the study used simplified imperfection shapes.

Study Limitations: The study acknowledges several limitations:

- Focus on specific methodology and structural types.
- Exclusion of welding details and their impact.
- Simplified approach to initial imperfections in buckling analysis.
- Lack of consideration for material and manufacturing variations.

Overall, the study provides valuable insights into the potential of high-strength steel for reducing weight in ship structures. However, further research is needed to address the limitations identified and develop a more comprehensive understanding of the complex factors involved.

2 Methodology

This project is an innovation project with participation from industrial partners and is contributing to the overall goal of sustainable shipping by proposing an improved design of the ship structures making use of extra high tensile steels. We focus on an electrically powered Ro-Pax ship as the target vessel and aim to reduce the weight as much as possible while keeping the structural strength, integrity and serviceability.

2.1 Buckling of stiffened panels

Buckling is one of the main failure modes in ship structures subjected to compressive loading and it is of crucial importance for the overall structural strength. In this study, we focus on buckling analyses of stiffened panels which form the basic building block and load-bearing element in ship structures. Various stiffened panel arrangements of a RoPax vessel are investigated. The analyses include the stiffened panels and also the surrounding structural members such as girders and frames. Different tools based on semi-analytical and numerical methods are compared, aiming for the establishment of a general assessment approach for such a problem.

Buckling is a phenomenon where structural members under compression loading deflect in an out-of-plane direction when the load reaches a critical value. After buckling, the deflection begins to increase in addition to the in-plane displacement, which leads to a reduction of in-plane or axial stiffness. Therefore, the load-carrying capacity of the structural member is decreased. This causes an increase of internal forces in unbuckled members, which may lead to progressive occurrence of buckling failure. If the load increases further, progressive buckling may result in the collapse of the whole structure. In general, ship structures are designed in a way that buckling collapse will occur in the secondary structural members such as plating and secondary stiffeners, rather than in primary structural members of frames, girders and bulkheads. About the buckling criteria, the first important remark is that elastic overall buckling of stiffeners is not accepted. However, elastic buckling of plating between stiffeners and girders is accepted as long as the stress re-distributions (load shedding) to neighbouring structures, such as stiffeners and girders, are insured.

The buckling of stiffened panels can be of various modes [5]. Buckling analyses involve considerations of all relevant buckling modes and their interactions. Mode interactions may be detrimental to the ultimate load-bearing capacity and will typically be pronounced in structures where two or more buckling modes will be triggered at or close to the same external load level. For stiffened plates, buckling is typically categorized into a local mode and an overall mode. The local mode, like plate buckling between stiffeners, involves a loss of stiffness and rigidity for the stiffener, which then triggers an overall mode which next amplifies the local mode etc. Mode interactions are also linked to load shedding between elements. In stiffened plated structures, a local plate buckling implies that the stresses shed to the surrounding structural members like stiffeners and the compressive loads then carried by the stiffeners amplify the plate deflections further.

In general, the buckling failure modes of a stiffened panel are split into the four following categories:

1) Plate buckling: plate buckling between stiffeners
2) Global buckling (also termed as overall buckling): lateral buckling of primary stiffener
3) Torsional buckling: sideways buckling of stiffener top
4) Web buckling: local buckling of stiffener web

In this study, all the above buckling modes are included in the buckling analyses. When stiffeners are strong enough so the overall buckling mode is prevented, the stiffened panel will buckle in local modes. These buckling patterns refer to the mode where either plating or stiffeners buckle separately. In addition, they can occur simultaneously at the same time and interact with each other. It is noteworthy that elastic buckling of plates which are properly supported around the edges displays positive post-buckling characteristics and loads beyond the eigenvalue can be carried.

2.2 Buckling analysis methods

Traditionally, the buckling strength has been assessed by rule formulas which are based on linear buckling theory in combination with some corrections to account for residual stresses, imperfections and plasticity. Although they provide quick strength estimations, they are very limited when dealing with complicated geometries, different load combinations, initial imperfections or geometric and material non-linearities. Thus, inaccurate results may be obtained due to the large influence that the previous phenomenon can have on the structural response when considered altogether. However, the rise in computational resources and tools has changed this trade providing a more consistent and accurate alternative approach than rule formulas.

2.2.1 PULS

However, it is not practical in terms of design and when a large number of structures are to be analysed as is the case of a shipyard. A current applied method for performing a fast buckling and ultimate strength assessment is PULS [6-7]. PULS is a computerized buckling code recognized by DNV and IACS (the International Association of Classification Societies) for strength assessment of stiffened thin plate elements as used in ship and offshore structures. The code is based on a direct semi-analytical approach using a recognized non-linear plate theory which is capable of predicting both the eigenvalues and the post-buckling behaviour up to the ultimate strength limit.

The code is developed and tailor-made for the purpose of doing fast buckling and ultimate strength assessments of local stiffened panels with an accuracy close to what is available using more advanced non-linear FE tools. The elements available cover the same structural layout as more standard closed-formed formulas, i.e. regular stiffening arrangements, etc., but have some extra features. The approach has the same theoretical basis as non-linear FE programs, which means that the results focus on concepts such as load-bearing capacities, elastic buckling eigenvalues, and plate deformations at collapse. Even though PULS provides more accurate results than simplified formulations with more efficient and cheaper computation costs than numerical methods, it has limitations in the applicable structures. For example, some large deck structures are composed of

more levels of stiffeners, which makes them difficult for PULS to handle. More details of this code are presented in the following. The strength assessment can be performed for combined loading as indicated in Figure 2-1, with the following loads taken into account:

- In-plane axial load in the direction of the stiffener, compression, or tension (σ1)
- In-plane transverse load in the direction perpendicular to the stiffener, compression, or tensions (σ2)
- In-plane shear (σ3)
- Lateral pressure

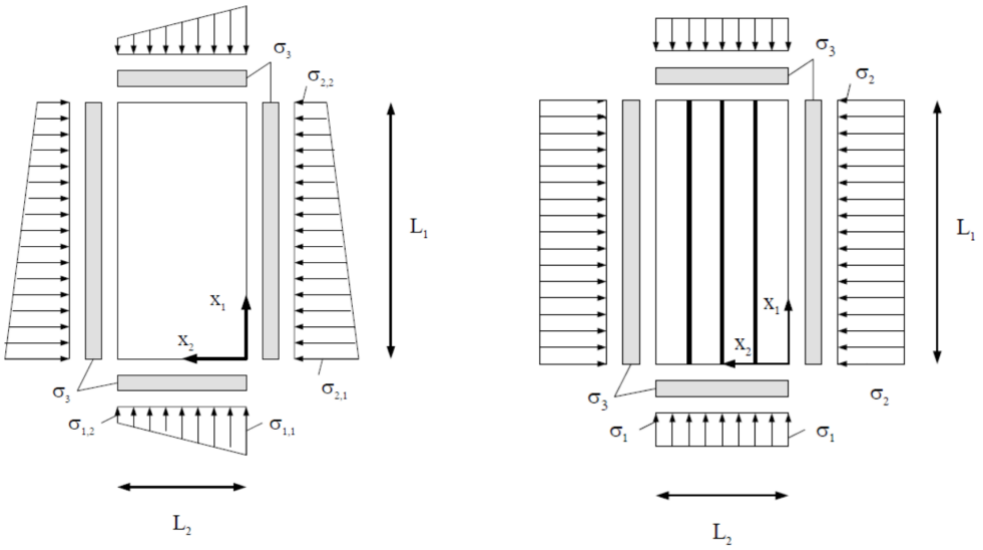

*Figure 2-1: Schematic combined loading [**Error! Bookmark not defined.**] for unstiffened plate (left) and stiffened panel (right)*

PULS's library contains four different structural elements, covering the regular stiffening, the non-regular stiffening, and the corrugation arrangements as presented in [8]. They are implemented in DNV's NAUTICUS Hull program and the basic plate elements (U3, S3) are also available in Excel format, which offers an easy input of a large number of panels, and therefore makes parametric studies easier to perform.

- U3: unstiffened rectangular plate
- S3: uni-axially or orthogonally stiffened rectangular panel
- T1: non-regular stiffened plate
- K3: symmetric trapezoidal open corrugation

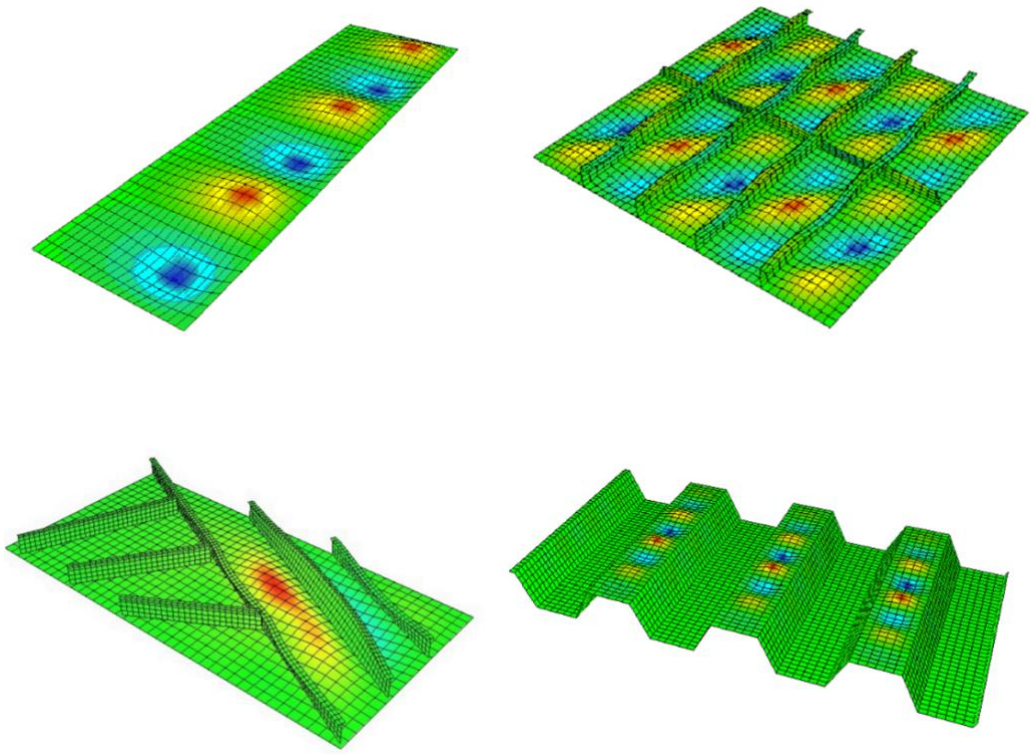

Figure 2-2: The four PULS elements [8]

In this work, PULS analyses were carried out with regard to both U3 and S3 configurations. In particular, stiffened panels (S3) are analyzed at a global and local level. Locally, the eigenvalue is evaluated for isolated component plates with a perfectly flat geometry; the buckling mode is used to set initial deflections, and post-buckling strength is estimated. At the global level, the stiffened panel is assessed in a way that considers the interaction between local and global modes. Regarding the initial imperfections, PULS automatically implements model tolerances based on standard fabrication practices for welded integrated structures used in ship-building and the offshore industry. According to the structural configuration, different imperfection amplitudes are considered.

2.2.2 Finite Element Analysis

The state-of-the-art analysis of the buckling analysis procedure is the numerical approach, represented by the Finite Element Method (FEM) and Finite Element Analysis (FEA). The numerical method accounts for the phenomena that rule formulas and semi-analytical tools cannot handle. This powerful tool has the main drawback of the significant modeling and computation costs. There are different complexities of buckling analysis using the FEA approach. DNV [9] proposes three different levels of FEA for carrying out buckling assessment:

- Linearized approach: Apply the FE method for assessing the buckling eigenvalues (linear bifurcation analysis) and determine the ultimate capacity using empirical formulas.
- Full non-linear analysis using code-defined equivalent tolerances and/or residual stresses.

- Non-linear analysis that is calibrated against code formulations or tests. Either of these methods can be used to determine the resistance of a structure or part of a structure and recommendations for their use are given in the following sections. The proposed methods are valid for ordinary buckling problems that are realistically described by the FE analysis.

In this work, both PULS and FEA are utilized for the buckling analyses. The FEA simulations of buckling and fatigue assessments are carried out in the commercial FE software ANSYS and Altair OptiStruct (Optimization-enabled Structural Analysis). Using ANSYS and Optistruct, both the linearized approach and the full non-linear analysis were investigated for the buckling assessments. This work aims to investigate and identify suitable tools for the objectives of weight-saving design concerning introducing Extra High Strength Steel (EHSS) and keeping the strength and serviceability of the vessel in structural terms. More details of the considerations and assumptions of the PULS and the FEA methodology will be discussed further in the next section of the report.

2.3 Initial imperfection

The buckling capacity of a stiffened panel is decided by the factors of structural geometry, material properties, loading characteristics, and boundary conditions. **In addition, initial geometrical imperfection is another key factor to be considered.**

Real structures do always have deviations from the perfect form due to welding and production etc. These imperfection patterns will be rather random and exact information is never available. In practice, shipyards and Class Societies have quality standards defining simple and local maximum tolerance limits to be measured over defined gauge lengths.

During the fabrication of a stiffened panel, the stiffeners in both directions are fitted into the plate by welding. Due to thermal effects, this process introduces initial imperfections and residual stresses into the structure, which tend to reduce the buckling and ultimate capacity of the element, hence it is important to know which shape and magnitude is to include them as an influencing parameter in design or analysis processes.

Different efforts have been made to study and predict the initial imperfections on a theoretical and numerical basis. However, due to the complexity of the phenomena and that the effect produced is normally of secondary interest approximate methods based on measurements are usually applied. Stiffened plate panels possess an extensive degree of redundancy in the ability to transfer induced membrane stresses to neighbouring frames and girders. A certain degree of initial out-of-flatness is not critical regarding the ultimate capacity. Normal production levels will typically give a scatter of capacity in the range 5−15%, [9]. However, the sensitivity and instability must be mapped in order to identify critical combinations of loading and boundary conditions and imperfection geometry.

The application of initial imperfections in design is characterized by great uncertainty. Thus, imperfection sensitivity is a hot topic. Typical imperfection patterns seen in the fabrication of stiffened plate panels are quite randomly distributed. Such geometries are inconvenient to model and exact data are not available (however, this work has not made use of FE software that can generate a stochastic imperfection FE model).

A simplified imperfection model is required concerning an efficient application and realistic strength predictions. However, some knowledge about relevant fabrication shapes should be retrieved in order to balance the modelled deflection according to the expected imperfection.

Considering the buckling strength, imperfection modes that coincide with the structure's own preferred deflection shapes are most unfavorable. A common and conservative approach is to set off the minimum eigenmode, which generally results in a reduced ultimate capacity.

An eigenvalue analysis is conducted prior to the strength analysis in order to obtain both elastic buckling stresses and eigenmodes. If the eigenvalues corresponding to the lower eigenmodes are clustered together, the structure will be prone to mode snapping [10]. In this case, a measured imperfection shape may be obtained by combining the corresponding eigenmodes.

Despite the unpredictable behaviour of the initial imperfections, it is commonly accepted that a symmetrical distribution of deflections where the plating between stiffeners deflects upwards, known as Hungry-Horse (HH) mode and illustrated in Figure 2-3, is suitable for the assumed pattern of the initial imperfection.

The HH mode tends to appear in the stiffened panel when a large lateral pressure is applied. This imperfection mode will in most cases introduce stiffening effects and add to the strength of the structure. It may, however, also entail mode-snapping effects due to the out-of-mode configuration for longitudinal compression. An alternative to the conventional implementation of imperfections is a weighted combination of the eigenmode and the HH-deflection.

This may give a more realistic deflection pattern and less conservative strength estimation. In this work, we make use of the tools of PULS and ANSYS, in which the influence from initial imperfection can be considered. For the FEA, the phenomenon of hungry-horse (HH) is taken as the initial imperfection. More details of this part will be presented in Section 3.

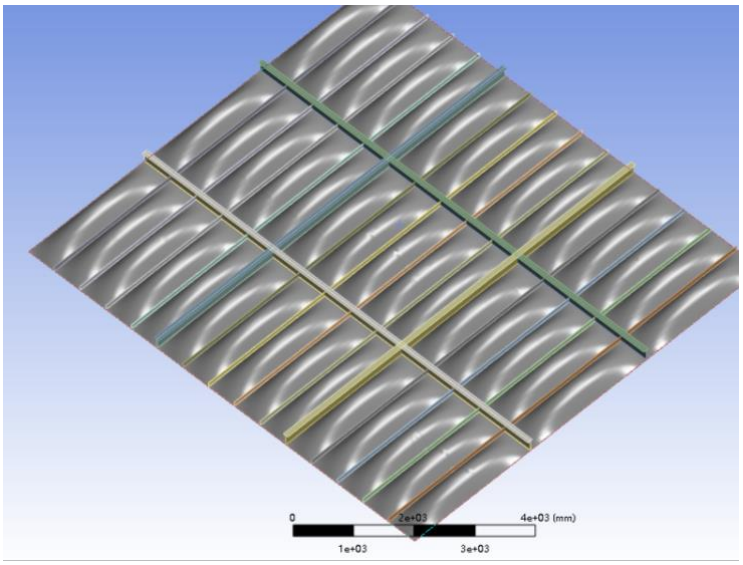

Figure 2-3: Illustration of a stiffened panel with a Hungry-horse (HH) initial imperfection

2.4 Material

In this work, we included two different sheets of steel and compared structures made of the two material properties. The hypothesis in this work is that the baseline designs are made of high-strength steel with a yield strength of 355MPa, which is termed HT36 in this work. HT36 is taken as the baseline material. The new designs are made of extra high-strength steel with a yield strength of 690MPa, which is termed HT69 in this work. Such extra high-strength steel is uncommon in building commercial ships. This study uses SSAB's Strenx 700 (HT69) steel as the reference for the evaluated material STRENX 700 (HT69). Figure 2-4 compares the baseline to the selected material for evaluation. The data is suitable for structural analysis. For the finite element modelling, the strain-stress curves of the two steels are simplified as bilinear, which are illustrated. The elastic modulus and the Poission'r ratio of both materials are assumed to be 200GPa and 0.3, respectively. It needs to be pointed out that the strain-stress curves illustrated in Figure 2-5 are simplified and deviate somewhat from the true strain-stress behaviors of the baseline steel and the evaluated material.

Baseline material

- HT36 Carbon Steel
- Yield strength: 355MPa
- Tensile strength: 450-590MPa

Evaluated material

- Strenx® 700
- Yield strength: 650-700MPa
- Tensile strength: 780-930MPa
- Elongation: min14%
- Thickness range: 4-160 (130) mm
- Superior Bendability & Surface quality
- Weldability with excellent HAZ strength & Toughness
- High impact toughness

Figure 2-4: Mechanical properties of selected carbon steel materials

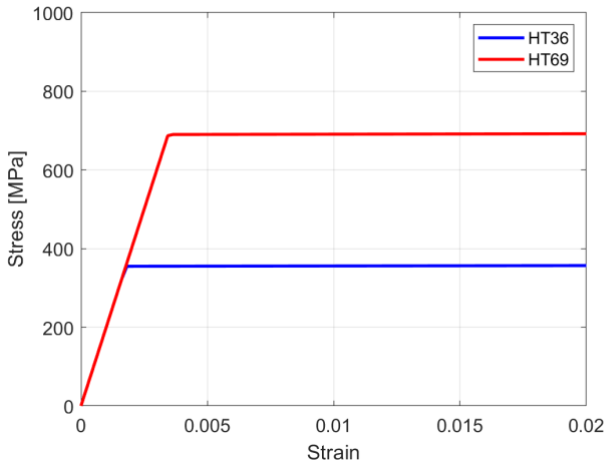

Figure 2-5: The strain-stress data of the baseline steel and the evaluated material

3 Optimization for deck structures

This section analyses a simplified main deck designed with two different steel grades. The two models will be compared using the methodology introduced in the previous section. The deck structure under analysis is the main deck of a RoPax ship, which is located approximately 3m above the waterline on the reference vessel.

- Investigation of the potential of weight reduction by using EHSS in RoPax deck structures
- Development of a practical method for structural design/optimization of ship deck structures. The following aspects are considered:
    - Optimization concerning weight, taking the increased tensile strength, buckling, and deflection as constraints.
    - Non-linear buckling behaviors with initial imperfection
    - Estimation of fatigue life reduction when introducing EHSS

3.1 Simplified stiffened panel

3.1.1 Model descritpion

We applied the above-mentioned PULS and FEA tools to a simple stiffened panel model and compared the results. This is mainly because PULS only handles models with limited complexity. The geometry dimensions of this simplified model originate from the main deck model, i.e., the criteria followed were the characteristics of the simplest structural element found in the later analyzed main deck model. This way, it is possible to investigate a complex structure from its most elementary component and thus understand its behavior in different designs. The dimensions of this model are listed in Table 3-1.

Table 3-1: Main dimensions of the stiffened panel.

Length [mm]	Width [mm]	Thickness [mm]	Web height [mm]	Web thickness [mm]
2400	3100	6	150	10

In this study, the deck structures' relative load-carrying capacity influenced by the different materials are investigated. We focus thus on the static loads. These include the weight of cargo and the structure, and the compression loads applied on the boundaries of the deck structures, in particular in the longitudinal direction.

Limitation: This analysis is limited to the investigation of buckling modes under static loads. The effects of tension loads due to global bending and torsional moments, while potentially significant, have been neglected in this study. This simplification is based on the assumption that these loads have a less significant impact on the load-carrying capacity of the structure when considering the change of materials. However, future studies may consider a more comprehensive analysis that includes these effects to provide a more accurate assessment of the structural behavior.

3.1.2 Boundary conditions

The boundary conditions can be divided into first- and second-order supports. Rotational edge supports are the first order, influencing mainly the elastic buckling stress and the ultimate capacity, whereas the second-order in-plane supports also have impacts on the post-buckling behaviour. In this study, we are more interested in the first-order boundary conditions. Figure 3-1 illustrates the configuration as well as the boundary conditions of the simplified stiffened panel model. In addition, a coupled behaviour was applied in the edges of the model to properly implement the model's restraints, i.e., so that the ends of the model remain straight.

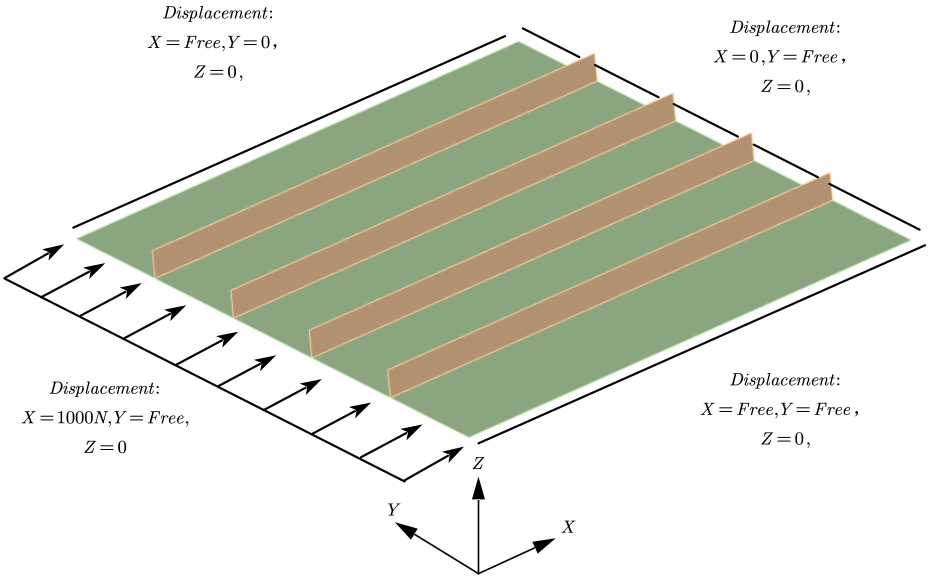

Figure 3-1: Illustration of the loading case for the deck model

3.1.3 Meshing

As mentioned in the methodology section, ANSYS is the code used to carry out the FE analyses. For all FE simulations, a mesh convergence study has been carried out to reach a reasonable mesh size concerning both accuracy and computation expenses. A mesh convergence involves systematically refining the mesh and gradually increasing the number of elements until the solution reaches a state of convergence.

The goal is to determine the optimal mesh density that produces consistent and stable results, reducing the dependence on the mesh size. The mesh convergence results for the stiffened panel model can be found in Table 3-2. We ran static/eigenvalue analyses in ANSYS, starting from a coarse mesh of 150mm until the finest mesh size of 25mm. The meshes turned convergent rather quickly. The deviation from the previous solution is 5% at most for the coarser mesh, reaching a magnitude below 1% for the finest mesh tested.

Table 3-2: Mesh convergence results for the stiffened panel.

Element size [mm]	150	100	75	50	25
Load Multiplier [-]	1.083	1.025	1.009	0.9902	0.9869
Applied load [MPa]	97	97	97	97	97
Elastic buckling stress [MPa]	105.1	99.40	97.81	96.22	95.73
Deviation from previous solution [%]	-	5.374	1.591	1.637	0.5111

Figure 3-2 shows the converged mesh of the simplified panel model, i.e., with a mesh size of 25 mm. This implies that there are six elements along the web of the stiffeners, which is in line with the FE theory regarding numerical accuracy.

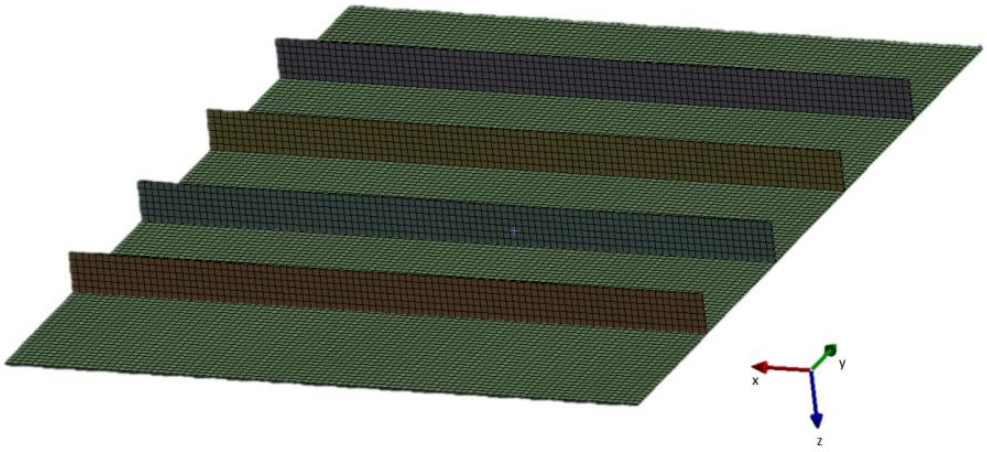

Figure 3-2: The mesh size after the convergence analysis.

3.1.4 Linearized buckling

The first local buckling stresses from the linearized FEA are compared with those from PULS. Two loading cases are studied: Case 1 is when the in-plane compression loads are applied in the longitudinal X-direction, and Case 2 is when the in-plane compression loads are applied in the transverse Y-direction. In addition, to evaluate the robustness of the tools, we have also added two plate thicknesses, 12 mm, and 15.5 mm, so that we have three different plate thicknesses in total.

The buckling modes are illustrated in Figure 3-3 and Figure 3-4 for the two loading cases, respectively. The buckling stresses are listed in Table 3-3. It is observed that the buckling eigenvalues calculated from ANSYS and PULS are very close for all the plate thicknesses and loading cases.

This implies PULS as a semi-analytical tool is suitable for buckling analysis of panels of this level of structural complexity. The numerical results show the local buckling of the plate and stiffener; this buckling mode is commonly referred to as the failure of a stiffener plate caused by a stiffener.

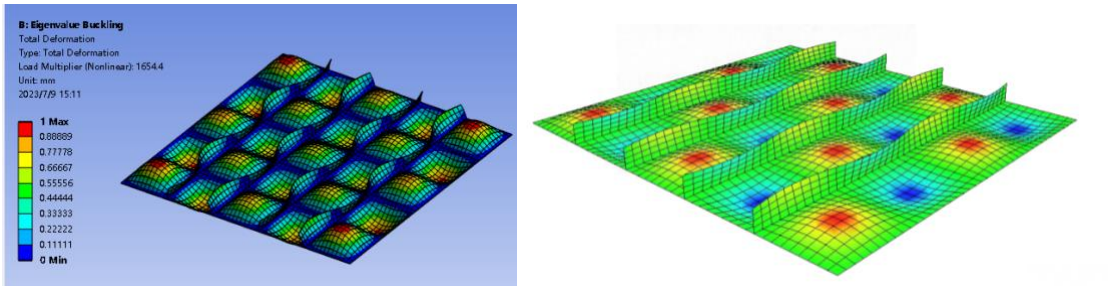

Figure 3-3: First local buckling eigenmode from linearized FEA (left) and PULS (right) under the in-plane loads from the longitudinal X-direction.

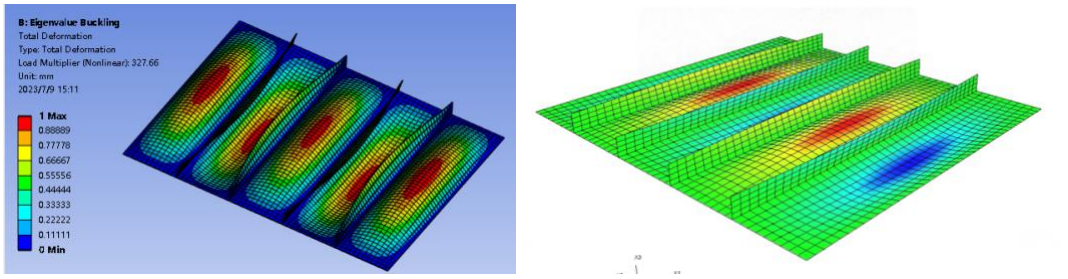

Figure 3-4: First local buckling eigenmode from linearized FEA (left) and PULS (right) under the in-plane loads from the transverse Y-direction.

Table 3-3: First local buckling stresses in MPa from linearized FEA (ANSYS) and PULS under the in-plane loads from the Y-direction.

Plate thickness	6mm		12mm		15.5mm	
	Case 1	Case 2	Case 1	Case 2	Case 1	Case 2
ANSYS	76	20	293	80	363	135
PULS	79	20	292	80	372	135

3.1.5 Load-carrying capacity

In addition to the linearized buckling analysis, we studied the load-carrying capacities of the simplified panel model with the increase of the plate thickness. This work is carried out through non-linear FE simulations using ANSYS, to understand how much the load capacity will be influenced by the plate thicknesses. Similar to the above-linearized buckling analyses, the loads are applied from the longitudinal and transverse directions, respectively.

Figure 3-5 and Figure 3-6 show the results. It is observed that the load-carrying capacities improve with the increase of the plate thickness. This phenomenon is almost linear in the longitudinal direction which is stiffened. However, the improvement of load-carrying capacity is less significant in the longitudinal direction in comparison with the transverse direction. In other words, the load-carrying capacity in compression in the longitudinal direction is less influenced by the reduction of the plate thickness.

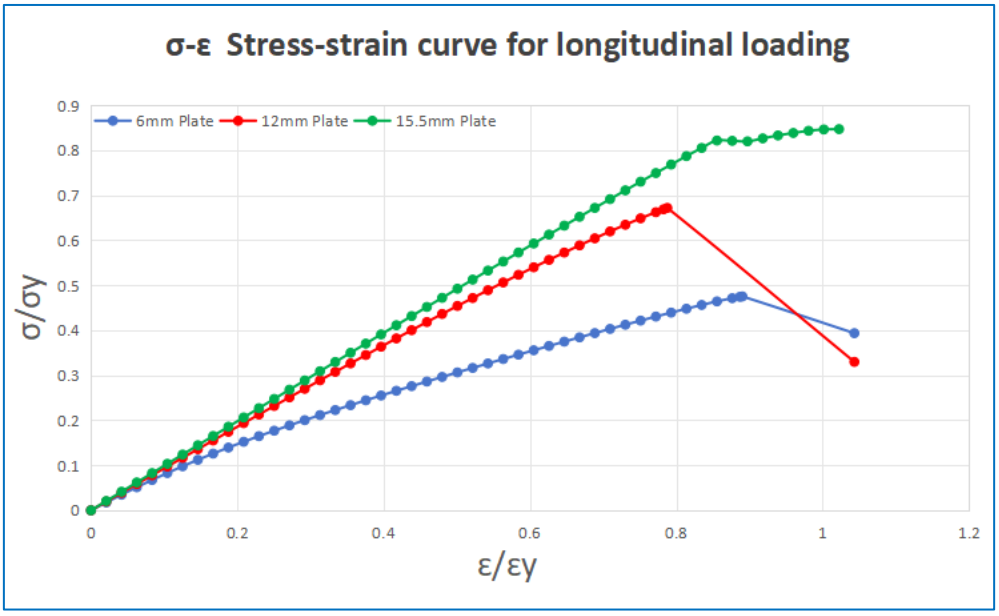

Figure 3-5: Non-linear FEA - Loading capacity under the in-plane loads from the X-direction.

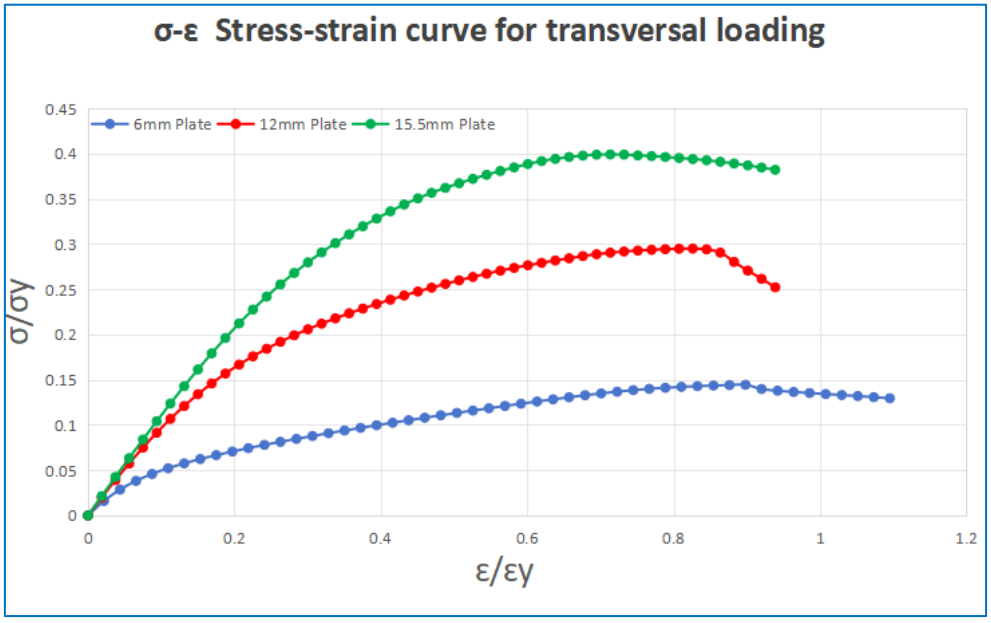

Figure 3-6: Non-linear FEA - Loading capacity under the in-plane loads from the Y-direction.

3.2 Multi-bayed panel

3.2.1 Model description

The simplified stiffened panel presented in the previous sub-section is only composed of the deck plate and the stiffeners in the longitudinal directions. In reality, a deck structure comprises multiple such simple panels that are integrated at the border by stronger stiffening structural members in both the longitudinal and the transverse directions.

Such a more complicated stiffened panel is termed a multi-bayed panel. Because multi-bayed panels often contain various sizes of supporting structural members, PULS can hardly be utilized to model in detail. In this work, we therefore only use the FEA tools for analysing the multi-bayed models.

A multi-bayed model following the typical configuration of the main deck of a RoPax is introduced. The panel is assumed to be located between surrounding heavier girders or stringers with a total length of 8100 mm and a total width of 9000 mm.

It spans over two transverse and two longitudinal T-shape girders. The stiffener spacing is 600 mm and the plate thickness is 10 mm. The main dimensions are visualized in Figure 3-7. Together the main dimensions, the configurations and dimensions of the stiffers and the girders are listed in Table 3-4. The material properties as well as the mesh sizing in the FE model follow the descriptions in Section 2.5 and Section 3.1, respectively.

Figure 3-7: Geometry model of the multi-bayed panel model

Table 3-4: Dimensions of the multi-bayed panel and the components.

Parameter	Dimension
Length [mm]	8100
Width [mm]	9000
Plate thickness [mm]	10
Stiffener Height [mm]	100
Stiffener Thickness [mm]	6

Stiffener Space [mm]	600
Stiffener Number	12
Longitudinal T-girder Web Height [mm]	200
Longitudinal T-girder Web Thickness [mm]	8
Longitudinal T-girder Flange Height [mm]	100
Longitudinal T-girder Flange Thickness [mm]	6
Longitudinal T-girder Number	2
Transverse T-girder Web Height [mm]	220
Transverse T-girder Web Thickness [mm]	10
Transverse T-girder Flange Height [mm]	100
Transverse T-girder Flange Thickness [mm]	8
Transverse T-girder Number	2

3.2.2 Boundary conditions and loads

The boundary conditions of the multi-bayed panel are similar to the simplified model. The outer boundaries of the model are simply supported and constrained to remain straight. These conditions are only applied to the border edges to ensure the central members are free to deform. Similar to the above-mentioned simplified stiffened panel model, boundary couplings are applied in the edges of the model to properly implement the model's restraints, i.e., so that the ends of the model remain straight.

Different from the simplified stiffened panel as mentioned in Section 3.1, in addition to in-plane loads, the multi-bayed panel model is also subjected to lateral pressure. The lateral pressure represents the deck loads in the vertical direction. For deck structures of a RoPax, the effects of lateral pressure together with the contribution to the initial imperfection must be carefully considered when analyzing the load-carrying capacity.

Regarding the applied loads, the classification rules [11] indicate the application of local loads for exposed and non-exposed decks. In particular, the static pressure (P_{dl_s}) shall not be taken less than 2.5 kN/m^2 for normal operations at the harbor, whereas such value differs for normal operation at sea, according to Equation 3.1 where (P_{dl_d}) stands for dynamic pressure, (a_z) is the vertical envelope acceleration and (g) is the acceleration of gravity.

$$P_{dl\_d} = (P_{dl\_s})x(1 + a_z/g) \tag{3.1}$$

In this work, we make use of non-linear FEA in ANSYS to study the effect of lateral pressure on the initial and load-dependent membrane stiffness, and the emergence of buckling mode is performed. The Hungry-Horse (HH) mode is taken as the initial imperfection. With the realistic stiffeners and girders modeled as constraints, the local buckling behavior is expected to be better captured. Material properties and mesh sizing are defined in similar ways in Section 3.1.

3.2.3 3.2.3 Introduction of Hungry-Horse (HH) imperfections

As mentioned in Section 2, we utilize the Hungry-Horse (HH) mode as the initial imperfections instead of the mode caused by eigenvalue buckling. In terms of buckling and ultimate strength, the deflections of greater influence are the angular change and the bending distortion since they lead to lower in-plane stiffness. Figure 3-8 illustrates an HH initial deflection with a scale factor of 100 of the multi-bayed panel. The HH initial deflections in the lateral z-direction are introduced in the deck plate following equations 3.2 and 3.3:

$$z = \omega_{max} \left| \cos\left(\pi\left(\frac{x+\frac{l}{2}}{l}\right)\right) \right| \cdot \left| \sin\left(\frac{\pi y}{s}\right) \right| \tag{3.2}$$

$$\omega_{max} = 0.005 \times s \tag{3.3}$$

where s is the longitudinal stiffener spacing, and l is the space between the transverse frames.

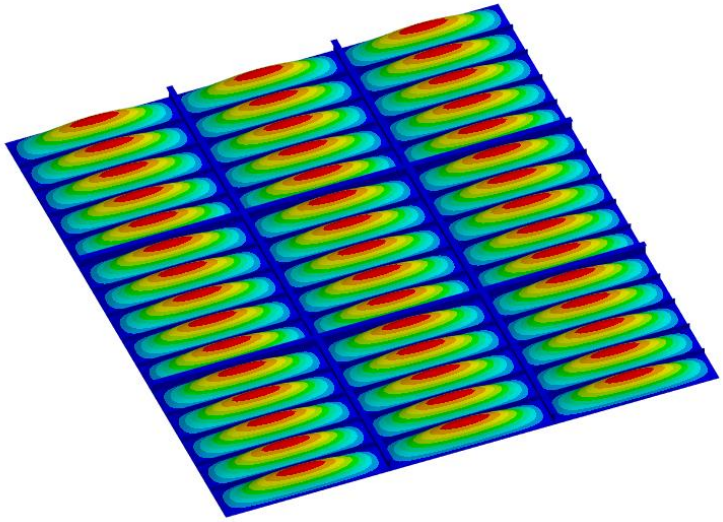

Figure 3-8: HH initial imperfection (Scale factor = 100) of the multi-bayed panel model.

Introducing in FE codes is however not straightforward because we need to define special field functions for the HH deflections and import the corresponding node displacements in the FE codes. In this work, we use ANSYS Workbench/Mechanical to incorporate the HH imperfections. The main procedure is presented as follows:

1) Create an input file using e.g. Excel. The input file is composed of three columns for the node displacements of X, Y, and Z. The numbers of the rows depend on the number of nodes in the finite element model. For the multi-bayed panel, approximately 10,000 rows are needed to match the nodes. More rows are possible and can be handled by ANSYS automatically through interpolation. However, more rows will result in unnecessary extra computation time. Please note the input file should be saved in CSV format. Figure 3-9 shows a part of the input sheet. It is observed that the values of the X and Y coordinates are supposed to match the element nodes, while the Z coordinates are calculated from Equation 3.1.

```
8100,8100,1.7634
8100,8150,2.4271
8100,8200,2.8532
8100,8250,3
8100,8300,2.8532
```

Figure 3-9:Example input file for the HH initial imperfection of the multi-bayed panel model.

2) In ANSYS Workbench, create a module of "External Data"; connect "External Data" to "Setup" of the "Static Structural" module; see Figure 3-10.

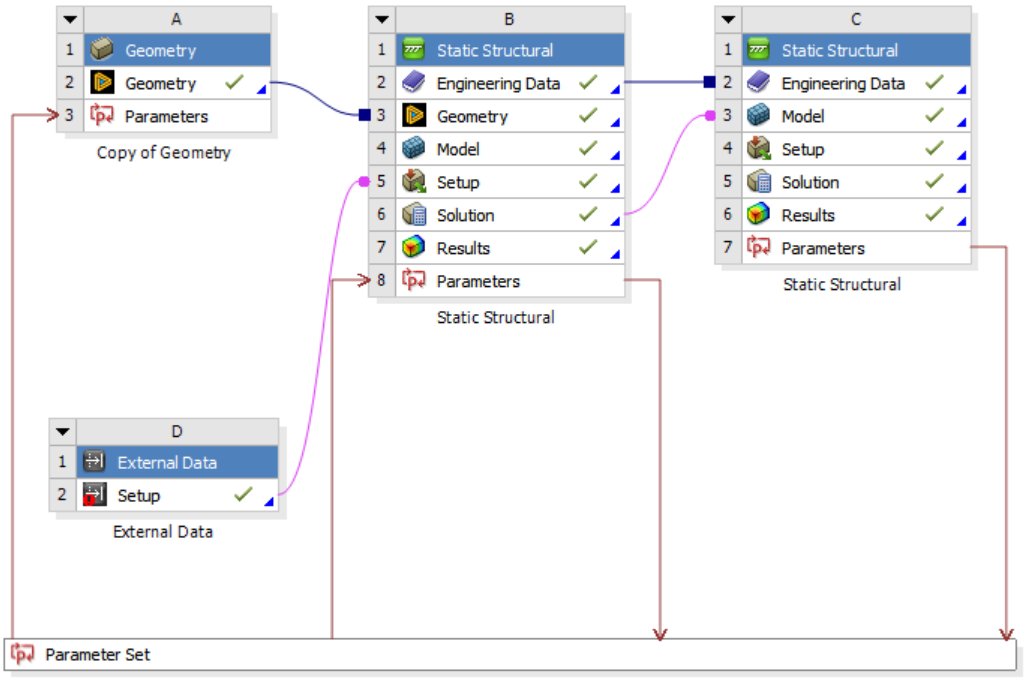

Figure 3-10: Non-linear buckling analysis in ANSYS when the HH imperfection is incorporated.

3) Read in the HH deflection input data. In ANSYS Mechanical when opening "Static Structural", click "Imported Load" and choose "Displacement"; by this operation, the HH deflections will imported as the node displacement. See Figure 3-11.

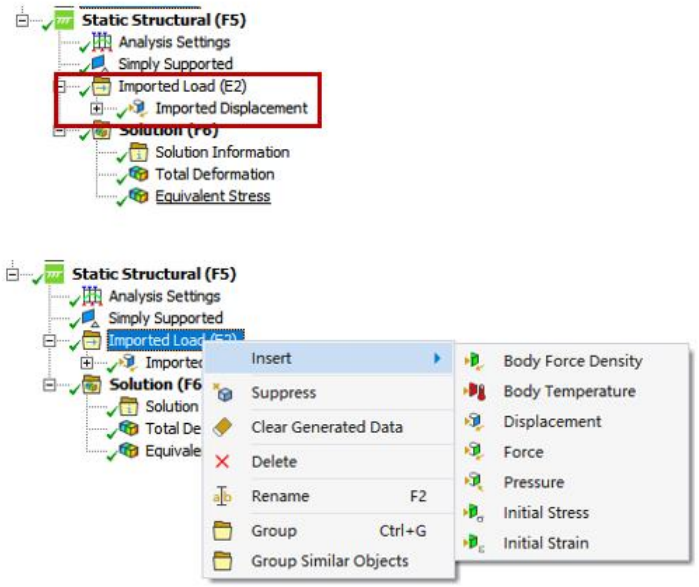

Figure 3-11: ANSYS Mechanical interface for importing the HH deflections.

3.2.4 Non-linear buckling with HH imperfection

With the HH deflections imported, we can now carry out non-linear buckling simulations using ANSYS for the multi-bayed model. We here apply an empirical lateral pressure of 5 kPa. The compression loads are applied as a predefined displacement of 50 mm in the -X direction. We defined two Steps: Step-1 is to apply the lateral pressure, while Step-2 is to apply the in-plane compression. 50 sub-steps are in use. It is noticeable that for a non-linear FE simulation, the Large Deflection option needs to be activated. See Figure 3-12 below for the ANSYS interfaces.

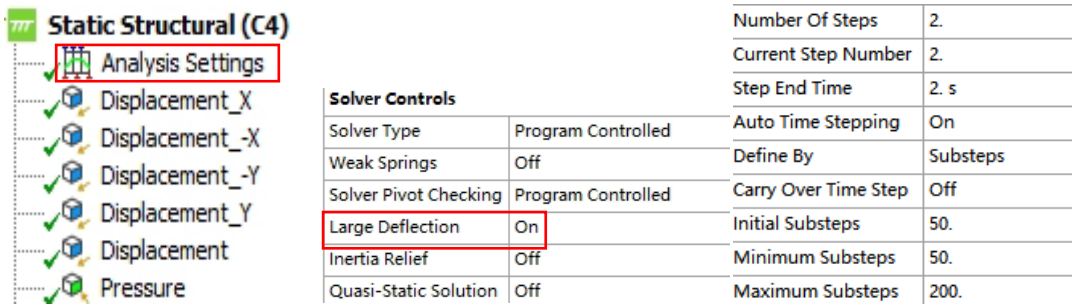

Figure 3-12: ANSYS Mechanical interface for importing the HH deflection – large defection option.

Under the combination of the above-mentioned loads and the initial HH-deflection, the multi-bayed panel model suffers from overall buckling. Figure 3-13 shows the Total Deformation after the overall buckling. It is observed that the largest deformation occurs on the plate in the middle of the panel structure. Lateral buckling is observed for the longitudinals in Figure 3-14, which is in line with the buckling mode shown in Figure 3-13.

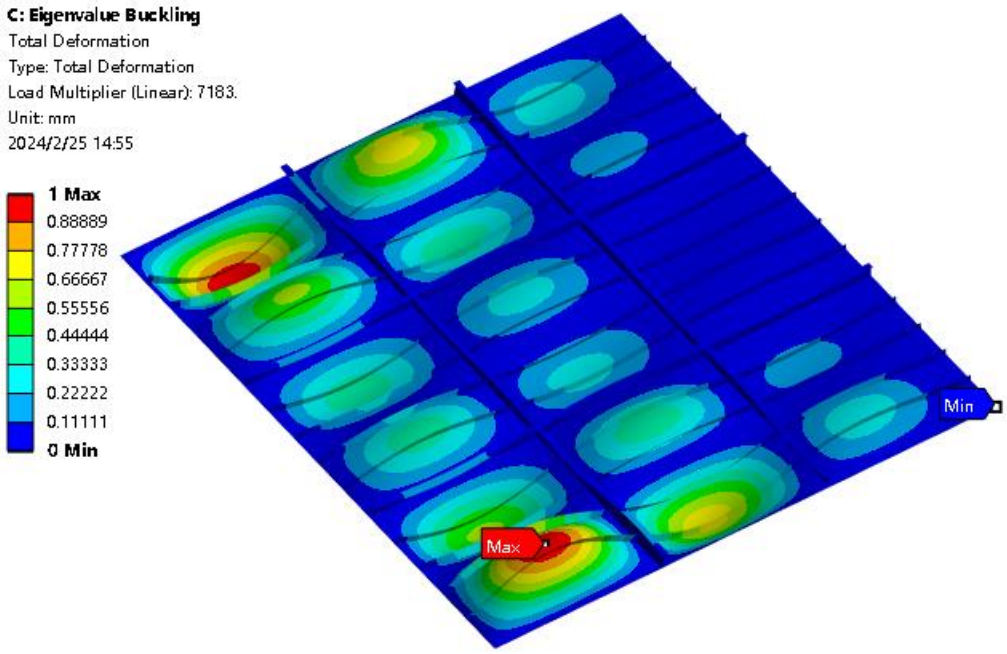

Figure 3-13: Overall buckling of the multi-bayed model from the non-linear FEA.

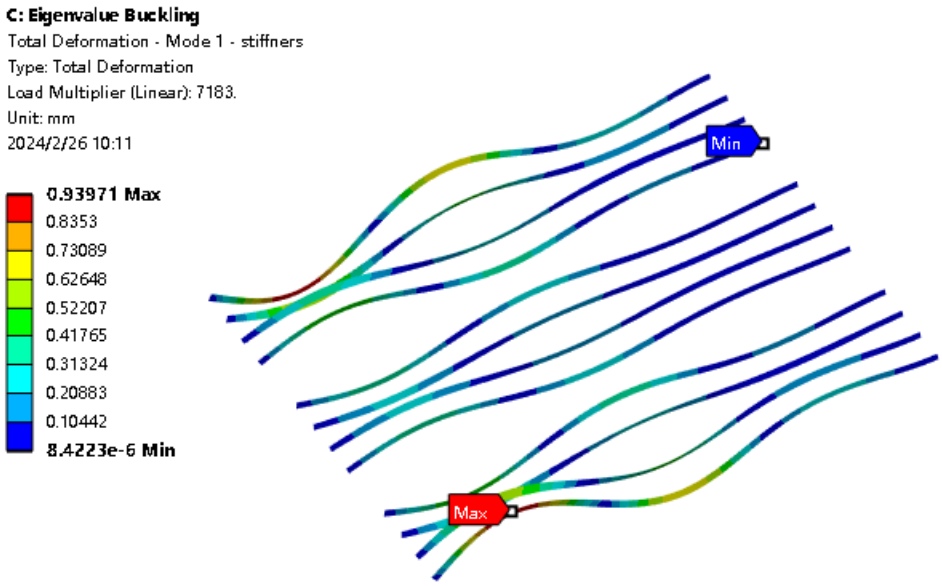

Figure 3-14: The deformation of the longitudinals when the overall buckling of the multi-bayed model occurs.

The above results are from the overall buckling, which is associated with the structure's ultimate strength and should be avoided by all efforts. In practice, we are more interested in local elastic buckling of the plate between the stiffeners. Such a plate buckling typically occurs under much lower loads and is the first sign that the deck structure begins to lose stability. We hereby compare plate local buckling for the multi-bayed model from both the approach of linearized buckling and the non-linear buckling method when the HH-imperfection has been introduced.

Table 3-5 presents the critical buckling forces of multi-bayed panels from different approaches. Similar to the above-mentioned loading cases, the in-plane buckling forces are applied in the -X direction, and the lateral pressure is set to 5 kPa. The critical buckling forces in MN are calculated for the materials HT36 (σ_y=355MPa) and STRENX 700 (HT69) (σ_y= 690MPa).

The first row in Table 3-5 lists the results for the eigenvalue bucking simulations. As expected, only increasing the material yield strength has little impact on the buckling limit. It is also observed that eigenvalue buckling might be over-conservative. The difference between the second and third rows is the imperfection mode.

It is found that the non-linear buckling limit when including HH-deflection is lower than that when the first eigenmode is assumed as the initial perfection, which implies that HH-imperfection is preferable if we need more realistic but still conservative buckling strength.

Table 3-5: Comparison of the buckling critical forces under a lateral pressure of 5 kPa of the multi-bayed panel from different approaches.

	HT36	**STRENX 700 (HT69)**
Eigenvalue Buckling [MN]	5.0	5.0
Non-linear buckling (Hungry-Horse imperfection) [MN]	8.3	8.7
Non-linear Buckling (first eigenmode) [MN]	17.1	17.0

3.3 Structural optimization

In this sub-section, we introduce a method to optimize the structure design from HTS to EHSS with the objective of minimization of the weight. The constraints are the material's yield strength, the structure's bucking capacity, and the limit of deflection. The weight optimization design is performed using ANSYS Workbench.

3.3.1 Parameterized FE modeling

To perform automatic optimization, we first need to convert the dimensions of the deck structure as well as the components into parameters. In this work, this is achieved through the ANSYS Workbench, with the modules SpaceClaim and Mechanical. The main steps of parametric modeling in SpaceClaim/Mechanical are presented as follows:

1) In SpaceClaim, through Design-Record-Script, activate the script recording feature; select the "Index" option. See Figure 3-15 below. By doing this, all our options in SpaceClaim will be recorded in this script.

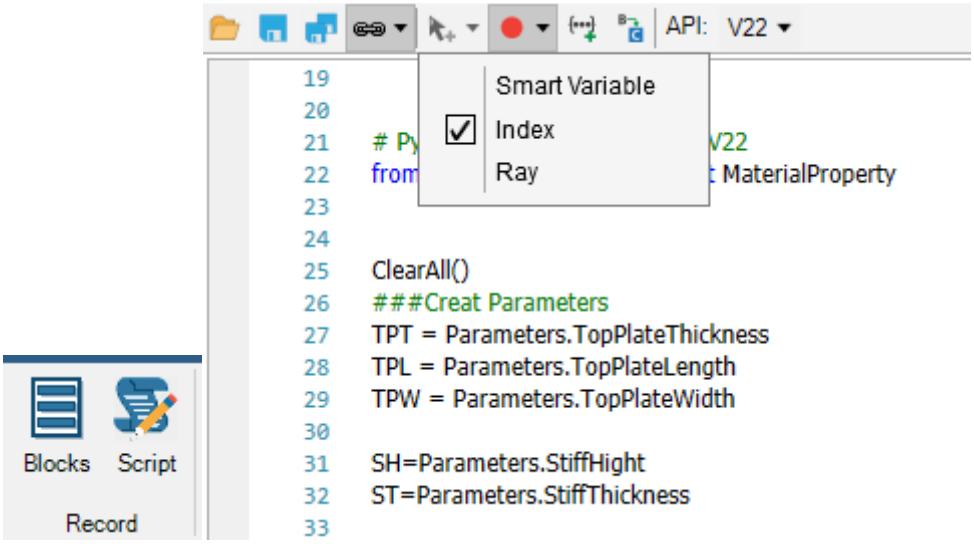

Figure 3-15: Creating script for parameterized FE modeling in SpaceClaim.

2) In the script, the parameters of various dimensions of the geometric model can be parametrized. In the script interface, one may create various variables and select those dimensions and even the number of the components as parameters to be optimized later on. For example, the parameters can be the plate thickness, number of the stiffeners, the height of the stiffener web, the thickness of the stiffener web, etc. Figure 3-16 shows some of the parameters of the multi-bayed model.

Figure 3-16: Example parameters of the multi-bayed model.

3) After creating a geometric model, using the script recording feature will automatically generate the corresponding code within the script. This code records the dimensions of the geometry and then replaces the previously established parameter values with specific size values. For instance, if the length parameter value for the panel, denoted as TPL, is 8100 mm for the plate model with the TPL parameter. After running the script, SpaceClaim will create a plate that is 8100 mm long. See Figure 3-17 for the example.

```
###Creat Parameters
TPT = Parameters.TopPlateThickness
TPL = Parameters.TopPlateLength
TPW = Parameters.TopPlateWidth
```

```
# Sketch Rectangle
plane = Plane.PlaneXY
result = ViewHelper.SetSketchPlane(plane)
point1 = Point2D.Create(MM(0),MM(0))
point2 = Point2D.Create(TPL,MM(0))
point3 = Point2D.Create(TPL,TPW)
result = SketchRectangle.Create(point1, point2, point3)
# EndBlock
```

Figure 3-17: Example of creating parameters in the SpaceClaim Script.

4) After creating the parameters in SpaceClaim, a "Parameter Set" will appear automatically in the interface of Workbenh, which is shared by the different modules of Workbench. The parameters created in SpaceClaim are the "Input Parameter" in the following modules Static Structural and Eigenvalue Buckling. See Figure 3-18.

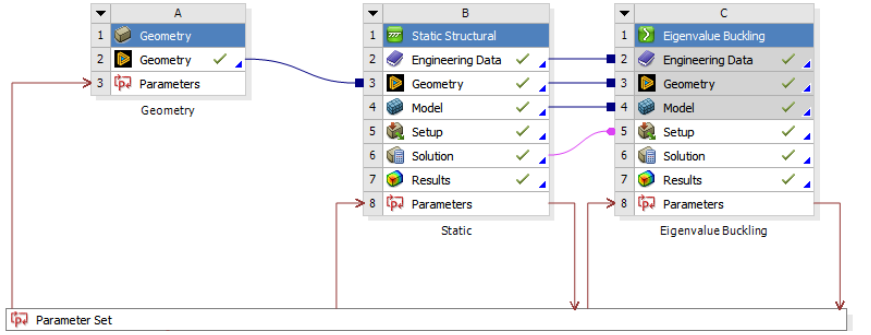

Input Parameters			
Geometry (A1)			
P84	TopPlateThickness	8	mm
P85	TopPlateLength	8100	mm
P86	TopPlateWidth	9000	mm
P87	StiffHight	110	mm
P88	StiffThickness	6	mm
P91	Long_Web_Height	200	mm
P92	Long_Web_Thickness	8	mm
P93	Long_Flange_Width	100	mm
P94	Long_Flange_Thickness	6	mm

Figure 3-18: Example of parameterization in ANSYS Workbench.

5) The Output Parameters can be defined in modules other than SpaceClaim. For example, because we want to include buckling strength as one of the constraints of the weight optimization, we choose Load Multiplier in the Eigenvalue Buckling module; see Figure 3-19.

P Load Multiplier	4996.6
Minimum	0. mm
Maximum	1. mm
Average	4.8772e-002 mm

Figure 3-19: Example of the selection of output parameter in ANSYS Workbench.

6) After the selection of the input and out parameters, ANSYS creates the Design Points; see Figure 3-20.

Name	P84 - TopPlateThickness	P85 - TopPlateLength	P86 - TopPlateWidth	P87 - StiffHight	P88 - StiffThickness
Units	mm	mm	mm	mm	mm
DP 9	10	8100	9000	100	6
DP 11 (Current)	8	8100	9000	110	6

P111 - Geometry Mass	P112 - LongWebs Stress Maximum	P113 - plate deflection Maximum	P114 - Total Deformation Load Multiplier	Retain
kg	MPa	mm		
5659.5	0.014201	1.5238E-05	4996.6	☑
6884.1	0.014024	2.0004E-05	7183	☑

Figure 3-20: Example of generation of the Design Point in ANSYS Workbench.

3.3.2 Response Surface Optimization

The optimization in ANSYS is performed based on the **Response Surface Methodology (RSM)**, which is also known as **response surface design**. This method utilizes a rational experimental design method to collect data through experiments. It employs a multivariate quadratic regression equation to model the relationship between factors and response values. By analyzing this regression equation, optimal process parameters can be sought, addressing multivariable problems. RSM is a statistical technique used to optimize processes by exploring the interaction effects of multiple variables.

Through a series of deterministic "experiments", RSM fits a response surface to simulate the true limit state surface. The fundamental idea is to assume an analytical expression involving unknown parameters for the limit state function in place of the actual, inexpressible structural limit state function. Response surface methodology combines statistical and comprehensive experimental techniques to address the impact of several variables on a system or structure.

Specifically, it deals with the transformation relationship between system or structure inputs (variable values) and outputs (responses). For illustration, consider a structural response Z with two variables, x1 and x2, having an unknown, inexpressible function relationship $Z = g(x1, x2)$. Obtaining the "true" function often requires extensive simulations. In contrast, response surface methodology approximates this relationship using a limited number of experiments to regress a function $Z = g'(x1, x2)$, which replaces the actual surface $Z = g(x1, x2)$.

This approach represents the functional response as a display function of basic random variables and is applied in reliability analysis. In practice, response surface methodology originates from an experimental design method. Experimental design methods are used to study the impact of design parameters on model behavior.

They determine the required number of sample points and their spatial distribution for constructing an approximate model. Two widely used experimental designs in computer simulation experiments are Latin hypercube sampling and uniform design. These methods are robust and applicable to various models, accommodating model variations.

We here use the example of the multi-bayed panel to demonstrate how the optimization is performed. As mentioned, the optimization objective is minimized weight when the material is changed from HTS to EHSS, while the buckling strength of the original design should be kept. In addition, we introduce two other constraints:

a) The material's yield limit should be utilized. When using STRENX 700 (HT69) , maximum allowable stress should be close to 230 MPa; we here make use of a factor of safety, FOS=3.
b) The maximum lateral deflection is another constraint. For the multi-bayed panel, we introduce an empirical allowable lateral deflection of 50 mm.

The optimization procedure in ANSYS is illustrated in Figure 3-21. We select four parameters as the Input Parameters to be optimized. It is possible to include more parameters for optimization. However, more parameters will result in a much longer computation time.

(1) the plate thickness
(2) the stiffener hight
(3) the stiffener thickness
(4) the number of the stiffeners

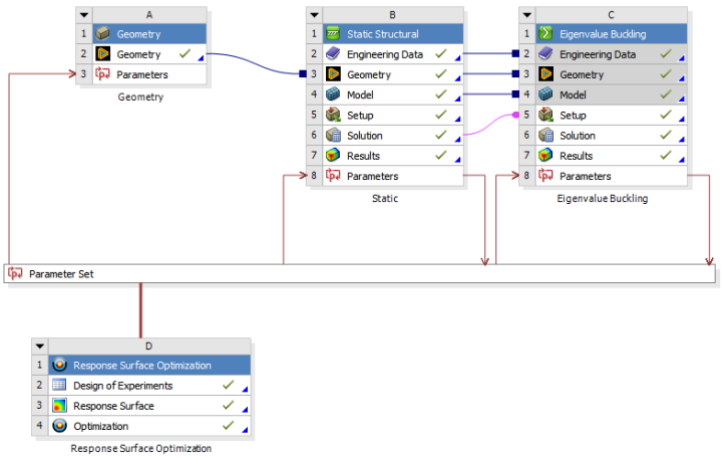

Figure 3-21: Example of an optimization procedure.

It is possible to define the range for the parameters. For example, we here limit the lower bound of the plate thickness to 8 mm. The optimization results are shown in Figure 3-22. Three candidates were proposed, which turned out to be similar to each other. The weight is reduced to about 5.6 tons with all the constraint values met. Table 3-6 lists the comparison of the original design of HT36 and the optimized design of STRENX 700 (HT69). It is observed that for the new design, the plate thickness is reduced to 8 mm, while the stiffener numbers are reduced to 9. The stiffener height is increased by 10%. The total weight is reduced by 18%, which should be considered a promising result regarding potential weight reduction. The geometry and the buckling mode of the optimized design are shown in Figure 3-23 and Figure 3-24, respectively.

Candidate Points

	Candidate Point 1	Candidate Point 2	Candidate Point 3
P84 - TopPlateThickness (mm)	8.0018	8.0025	8.008
P87 - StiffHight (mm)	109.53	109.32	109.04
P88 - StiffThickness (mm)	5.5449	5.5322	5.4906
P108 - Stiff_Nr_Total	9.473	9.7824	9.9729
P111 - Geometry Mass (kg)	× 5652.9	× 5660.3	× 5664.5
P114 - Total Deformation Load Multiplier	5001.9	5021.9	5005.1

Figure 3-22: Example of the optimized design candidates.

Table 3-6: Dimensions of the mult-bayed panel and the components.

Parameter	HT36	STRENX 700 (HT69)	Parameter value change
Length [mm]	8100	8100	-
Width [mm]	9000	9000	-
Plate thickness [mm]	10	8	-20%
Stiffener Height [mm]	100	110	+10%
Stiffener Thickness [mm]	6	6	-
Stiffener Space [mm]	600	600	-
Stiffener Number	12	9	-25%
Longitudinal T-girder Web Height [mm]	200	200	-
Longitudinal T-girder Web Thickness [mm]	8	8	-
Longitudinal T-girder Flange Height [mm]	100	100	-
Longitudinal T-girder Flange Thickness [mm]	6	6	-
Longitudinal T-girder Number	2	2	-
Transverse T-girder Web Height [mm]	220	220	-
Transverse T-girder Web Thickness [mm]	10	10	-
Transverse T-girder Flange Height [mm]	100	100	-
Transverse T-girder Flange Thickness [mm]	8	8	-
Transverse T-girder Number	2	2	-
Mass [kg]	6884	5660	-18%

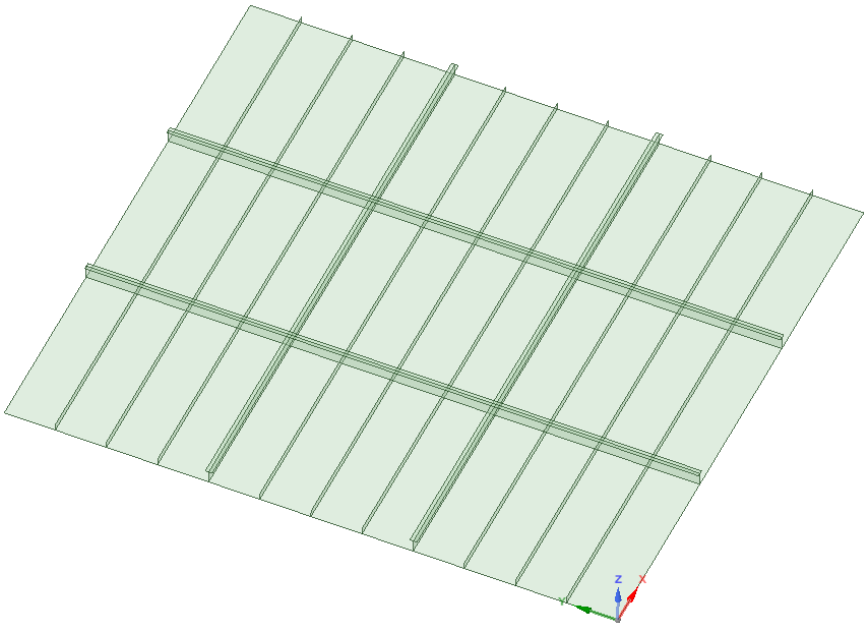

Figure 3-23: Geometry of the EHSS design of the multi-bayed panel.

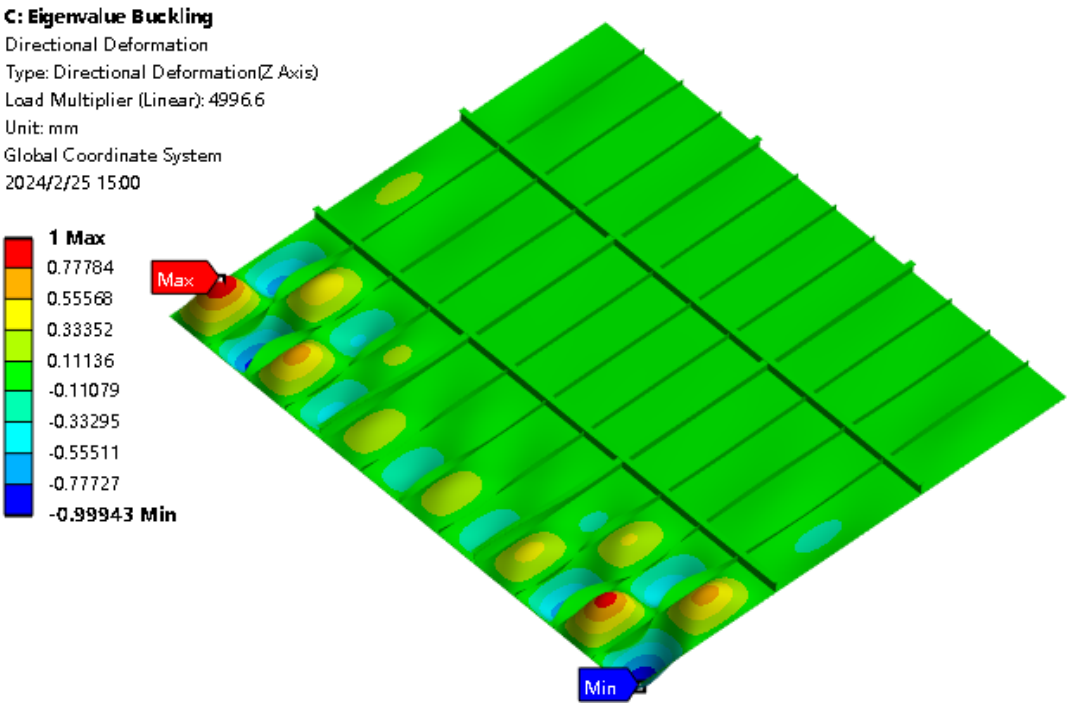

Figure 3-24: Buckling mode of the EHSS design of the multi-bayed panel.

3.4 Simplified fatigue comparison

It has been commonly accepted that introducing STRENX 700 (HT69) is disadvantageous for ship structural members. These increased stress levels in ship structural members are expected to result in reduced fatigue life. Measures must be taken to improve fatigue design. This requires first of all evaluation of the shrunk fatigue margin when the stress magnitude in the structures is increased when STRENX 700 (HT69) is introduced.

We made a simplified fatigue comparison of the two designs of the multi-bayed panel. The dimensions of the optimized panel using the evaluated material and the original panel using the the baseline material are presented in Table 3-6. It is assumed that both panels are subject to identical empirical pressure loads, which results in fatigue damages at the structural details when stress concentration occurs.

Fatigue damages are then calculated for the locations where the highest local stresses are found, according to the SN-curves recommended by classification guidelines. This simplified fatigue comparison meets the purpose of this study, which compares the fatigue performance when steels of higher tensile strength are introduced.

3.4.1 Stress-based fatigue

Fatigue methods are typically divided into three different methods: the stress-based approach, the strain-based approach, and the fracture mechanics approach, where the stress-based approach is the most common method for most engineering problems. Within the scope of the stress-based approach, a so-called method of hot-spot stress has been utilized in the shipbuilding industry.

A hot-spot stress is defined as a stress value obtained by extrapolating stresses at a certain distance from the weld toe based on finite element analysis. It is recognized that hot-spot stress values may vary for different elements and different extrapolation techniques. For this reason, we use instead local stress extracted from the structural details together with SN curves of nominal stress, because we aim in this project to compare designs of different steels.

The SN curves are associated with the theory of fatigue damage accumulation. The most widely recognized damage accumulation rule is the Palmgren-Miner rule [12], which states that the accumulated damage of a batch of stress cycles is the number of cycles that occurred divided by the number of cycles that would cause the material failure.

Failure is assumed when the accumulated damage equals to unit. Fatigue damage accumulation with the Palmgren-Miner rule may be carried out by estimating the linear cumulative fatigue damage D by using the Palmgren-Miner rule formulated as:

$$D = \sum_{i=1}^{n_{tot}} \frac{n_i}{N_i} \tag{3.4}$$

where:

n_i = Number of cycles at stress range $\Delta\sigma i$

N_i = Number of cycles to failure at stress range $\Delta\sigma i$

n_{tot} = Total number of stress range blocks

i = Stress range block index.

The number of load cycles, ni, is determined by the long-term stress distribution, e.g. represented by the Weibull distribution, while the number of cycles to failure, N_i, is represented by the SN curve. The acceptance criteria for damage D is given by the rules.

In this work, because the major aim is to compare different steel materials, we only consider the in-air environment. The corrosive environment as the mean stress effect, thickness effect, material effect, and the post-weld treatment, which have impacts on the fatigue strength of ship structures have not been taken into account. Besides, the scantling approach factor and the operational region factor which are mentioned in the DNV Class Guideline Strength analysis of hull structure in RO-RO vessels (DNV-CG-0137) are neglected.

3.4.2 Calculation of fatigue cycles

In this work, we establish a practical FEA-based approach to estimate fatigue damages of the multi-bayed panel structure of the original design of HT36 with the optimized design of STRENX 700 (HT69). We first introduced structural details that stress concentrations are accounted for to find out the local stress level.

Fatigue damages are then calculated making use of representative loading conditions to identify the fatigue critical locations. By this means, we derived the fatigue lives of the original design and the optimized design, following the DNV Class Guieline Fatigue Assessment of Ship Structures (DNV-CG-0129).

Fatigue damages are expected to accumulate at the locations where stress levels are significantly higher than in the surrounding locations. This phenomenon is termed as stress concentration. A stress concentration occurs typically at structural details with abrupt geometrical changes. For a deck panel, openings are needed at the intersection of the longitudinal stiffeners and the transverse girders. Stress concentration occurs typically at such a structural detail of opening.

Figure 3-25 illustrates the FE model of the structural details at the opening of the longitudinal/transverse intersections. Fine meshes with the element size at the level of plate thickness are in use at the locations where stress concentrations are expected.

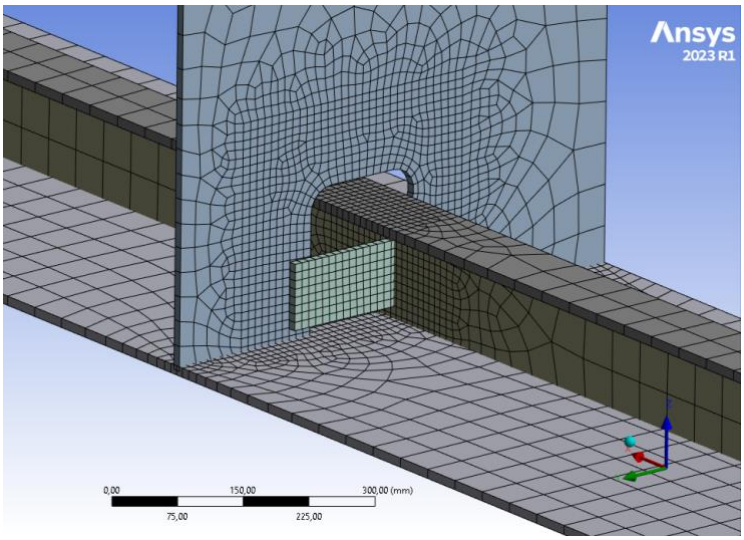

Figure 3-25: The local FE model for fatigue assessment.

In this work, we are most interested in the fatigue capacity of the base materials instead of the welded joints. We need thus first to find out the fatigue stress ranges at the critical structure details as illustrated in Figure 3-26 of the baseline materials of the different designs, based on which we can calculate the fatigue damages using the different SN curves. The fatigue stress range $\Delta\sigma$ is simplified and assumed to be caused by the pressure loads of 0.5MPa. Under such loads, the fatigue stress range is found as 155 MPa for the original HT36 steel design. While for the optimized STRENX 700 (HT69) steel design, the fatigue stress range increases to 265 MPa.

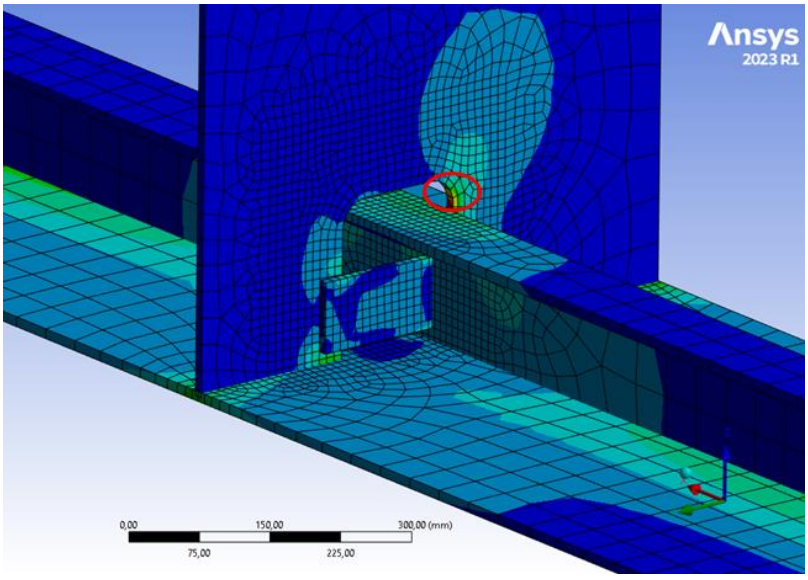

Figure 3-26: The fatigue-critical location of the baseline models.

Two different SN curves are in use for the HT36 and the STRENX 700 (HT69). For the original design of the HT36 steel, the SN parameters are assumed to follow the B2 curve of the recommended DNV SN curves DNV [13]; see the blue curve in Figure 3-27. This is a two-slope SN curve that applies to base materials in air conditions. The parameters in Eqn (3.5) are m=4 $\log(K_2) = 14.886$ for $N \leq 10^7$, and m=6 $\log(K_2) = 18.828$ for $N > 10^7$.

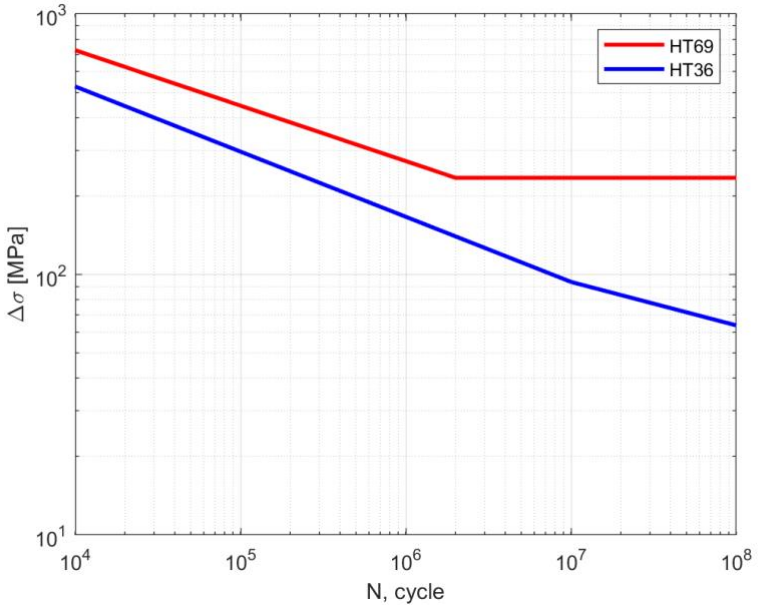

Figure 3-27: The typical SN curves for base materials in air [12]

$$\log(N) = \log(K_2) - m \cdot \log(\Delta\sigma) \tag{3.5}$$

These conventional recommended SN curves apply to steels with yield stress up to 500 MPa. For the STRENX 700 (HT69) steel design, however, those conventional SN curves become invalid. Another SN curve for base material is hence in use, which is also adopted from the DNV class guideline [13]. This new SN curve is illustrated as the red curve in Figure 3-27, for which the mean SN curve is given by $\log(N) = 17.770 - 4.7 \cdot \log(\Delta\sigma)$. It is observed that for this SN-curve in air, a fatigue limit at $2 \cdot 10^6$ cycles at a stress range equal to 235 MPa is assumed. Making use of these two SN curves, the failure cycles can be calculated based on the above-mentioned fatigue stress ranges. for the HT36 steel design, it is calculated that $N = 1.33 \cdot 10^6$; while for the STRENX 700 (HT69) steel design, $N = 1.14 \cdot 10^6$.

In other words, the failure cycles for the optimized design of extra high-strength steel are about 85% of the original design made of conventional steel, which should be considered acceptable concerning weight reduction.

3.4.3 An important remark

The above failure cycles are for comparison of the two designs of different materials regarding fatigue performance. We conclude that replacing the baseline steel with the higher strength steel leads to significant weight reduction. Meanwhile, the stress level at the structural details increases for the design of the evaluated material, leading to more fatigue damage. It is noteworthy that the structural details of the STRENX 700 (HT69) steel are kept unmodified as the HT36 steel.

In other words, we have not optimized the fatigue-critical locations concerning the increased stress level. Fatigue dimensioning of structural details is outside the scope of the current work.

We in this work proved that fatigue performance becomes crucial for ship structures when using higher strength steels. To calculate long-term fatigue damages as well as the fatigue life of ship structural components, we need to include more loading conditions and statistical fatigue assessments to account for the dynamic wave loads. Also, we need to establish additional global and/or partial FE models to fully consider the force combinations applied to the ship structural components, which can be part of future work following this project.

4 Analysis of car-deck

Car-decks are typical deck types for RoPax and PCTC ships. These decks can be adjusted to different heights, allowing for efficient loading and unloading of vehicles. A car-deck panel is a stiffened plate field of an open web construction, consisting of a top plate, main girders, secondary stiffeners, buckling stiffeners, brackets, and small boxes acting as supports. Figure 4-1 shows a typical car-deck panel designed by MacGregor Sweden AB, where the flanges are indicated with orange.

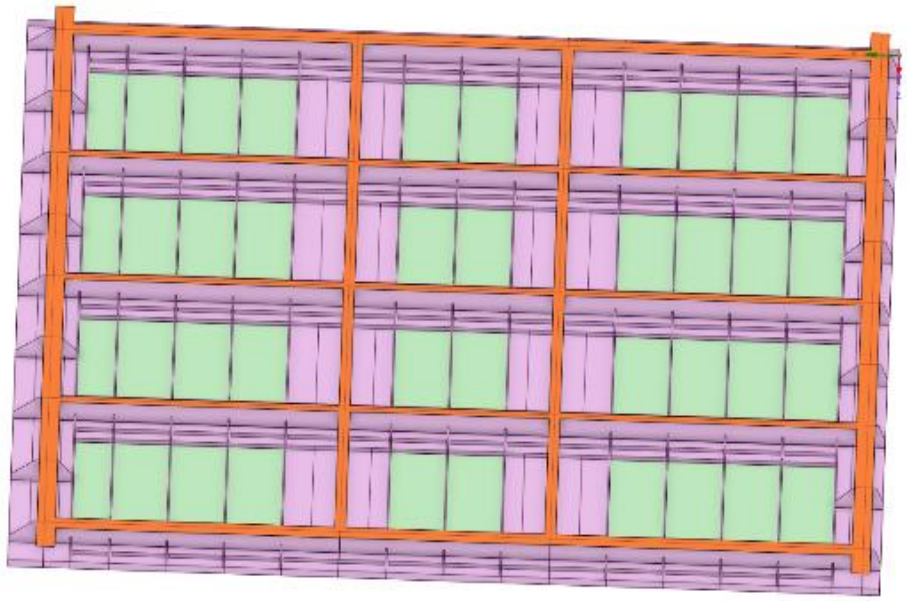

Figure 4-1. Typical car-deck panel

Typical loads of a car-deck are Uniformly Distributed Loads (UDL) with a typical range of 150-300 kg/m2 and axle loads with a range of 1-2 tons for each axle. The car-deck panel can be operated either with a Mobile Deck Lifter, a vehicle specially designed for this purpose, or with a fixed installed hoistable system. The support points are typically in the corners of the panel and if possible in between corners for a shorter free span.

This is highly dependent on the structure of the vessel's hull and the design of pillars to support the local deck and the global structure. Normally the deflection of the loaded panel structure limits the design. A specific building height is often reserved in the hull structure to allow a certain specified clear height below the panel. A higher building height or larger allowable deflection causes the vessel's total height to increase to keep the same load capacity.

4.1 Design comparison

In this section, MacGregor compared the design of the evaluated material with that of the baseline material. The general parameters of the car-deck panel of the original design using HT36 are illustrated in Figure 4-2. The dimensions are kept for the new design using Strenx 700 (HT69), but the steel thickness is cut off by ⅓, following SSAB's recommendation.

Example Panel: Wallenius - 4111566-F Cat A

- HT36
- L: 12,77 m
- B: 11,8 m
- H: 340 mm
- Top plate: 6 mm
- Flanges: 20 mm
- Webs: 6 mm
- Weight: 13 300 kg (7850kg/m3 density)
- UDL 300kg/m2
- Stiffener: HP100x6, Spacing 775 mm

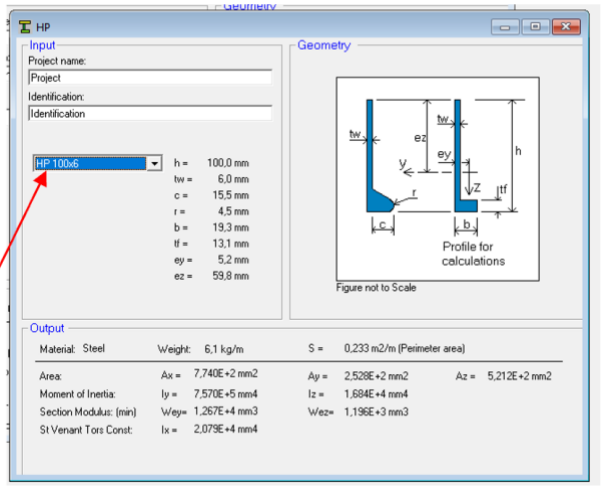

Figure 4-2. Dimension and main parameters of the car-deck panel

Table 4-1 presents the comparison of essential data for feasibility analyses and corresponding weight reduction. It is observed that significant weight reduction can be achieved by introducing the higher steel strength.

Table 4-1: Comparison of essential data for feasibility analyses and corresponding weight reduction.

	HT36	**Strenx 700 (HT69)**	**Unit**	**Remarks**
Area	247.1	247.1	m^2	
Volume	1.784	1.204	m^3	
Weight	14.0	9.45	Ton	32.5% weight reduction
Density	7850	7850	kg/m^3	
Top Plate (thickness)	6	4	mm	33% weight reduction
Top Plate (LxW)	12.77x11.80	12.77x11.80	m	
Flange	20	14	mm	(3.13ton vs 2.19ton) 30% weight reduction
Webs	6	4	mm	(1.68ton vs. 1.12ton) 33% weight reduction
HP100xtw	tw = 6	tw = 4	mm	(1.11ton vs. 0.75ton) 32% weight reduction

If this concept is applied to a whole vessel, for instance, a large PCTC, with 6 car deck levels and a total car deck panel area of approximately 22 000 m^2 and comparing the weights using Strenx 700 (HT69) material, there is a potential to save 626 tons of steel, which has a positive impact on the whole vessel's performance.

- 6 Decks with car deck panels
- Total car deck panel area: approx. 22 000 m^2

- HT36: 1 937 t
- Strenx 700 (HT69): 1 311 t
- Diff: 626 t

In addition to the weight, we also compared the stress and deflections of the two designs using different materials, which are illustrated in Figure 4-3, Figure 4-4, Figure 4-5 and Figure 4-6.

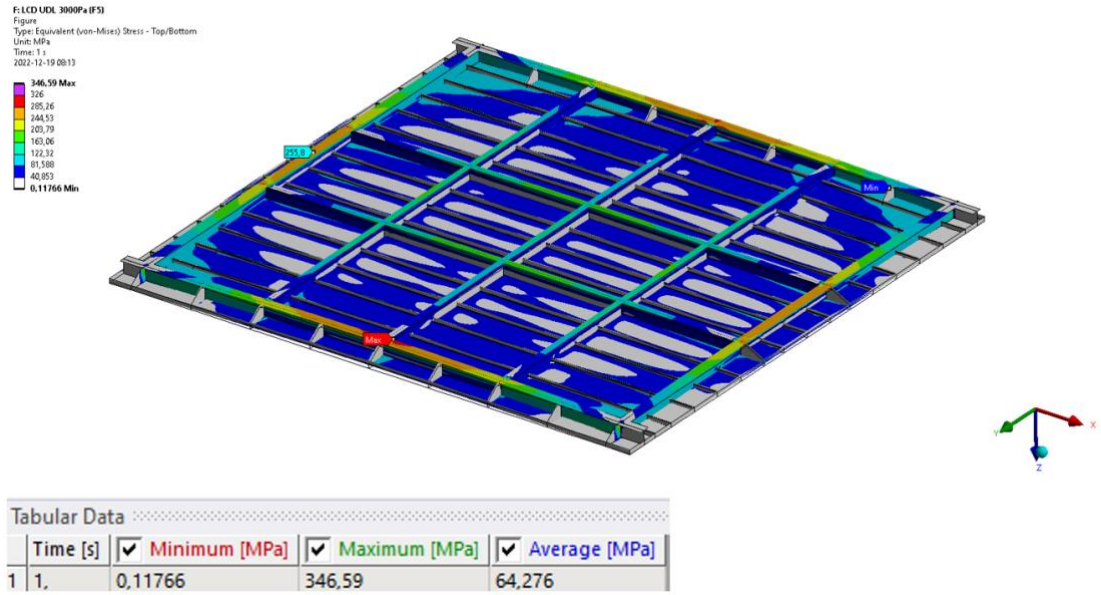

Tabular Data

	Time [s]	Minimum [MPa]	Maximum [MPa]	Average [MPa]
1	1.	0,11766	346,59	64,276

Figure 4-3. Stress plot of the original design of HT36

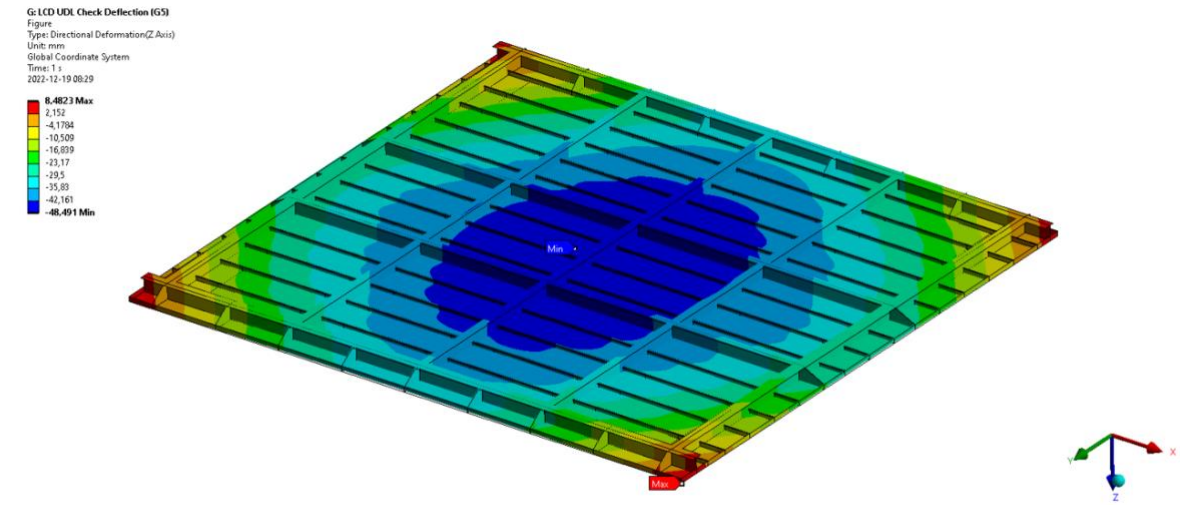

Tabular Data

	Time [s]	Minimum [mm]	Maximum [mm]	Average [mm]
1	1.	-48,491	8,4823	-30,618

Figure 4-4. Deflection plot of the original design of HT36

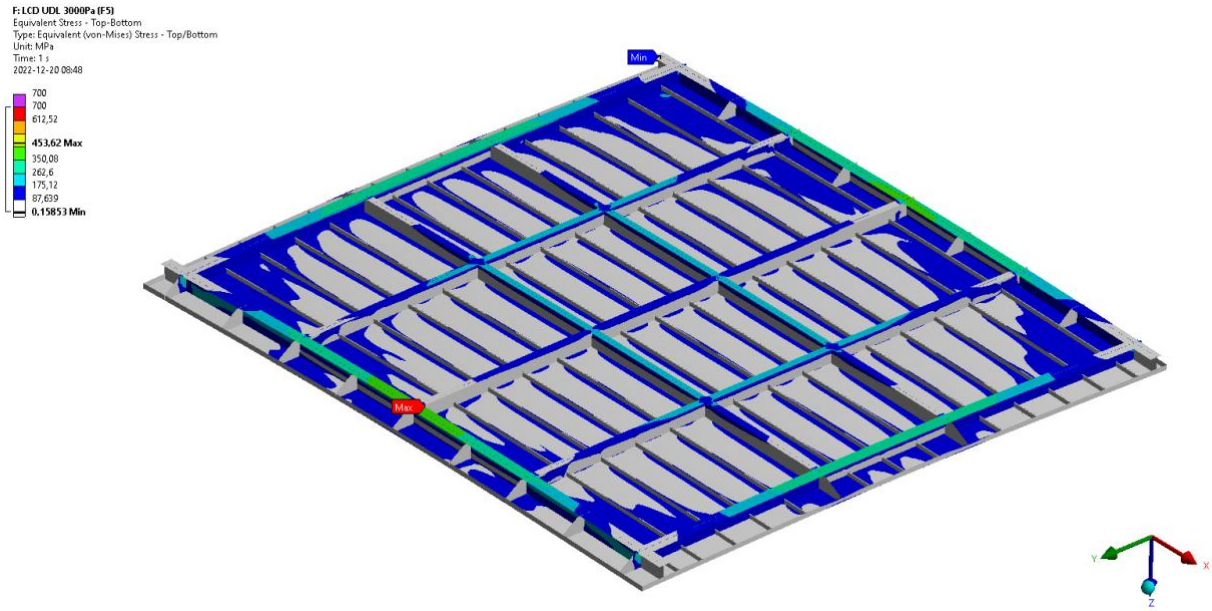

Tabular Data

	Time [s]	Minimum [MPa]	Maximum [MPa]	Average [MPa]
1	1,	0,15853	453,62	89,387

Figure 4-5. Stress plot of the new design of Strenx 700 (HT69)

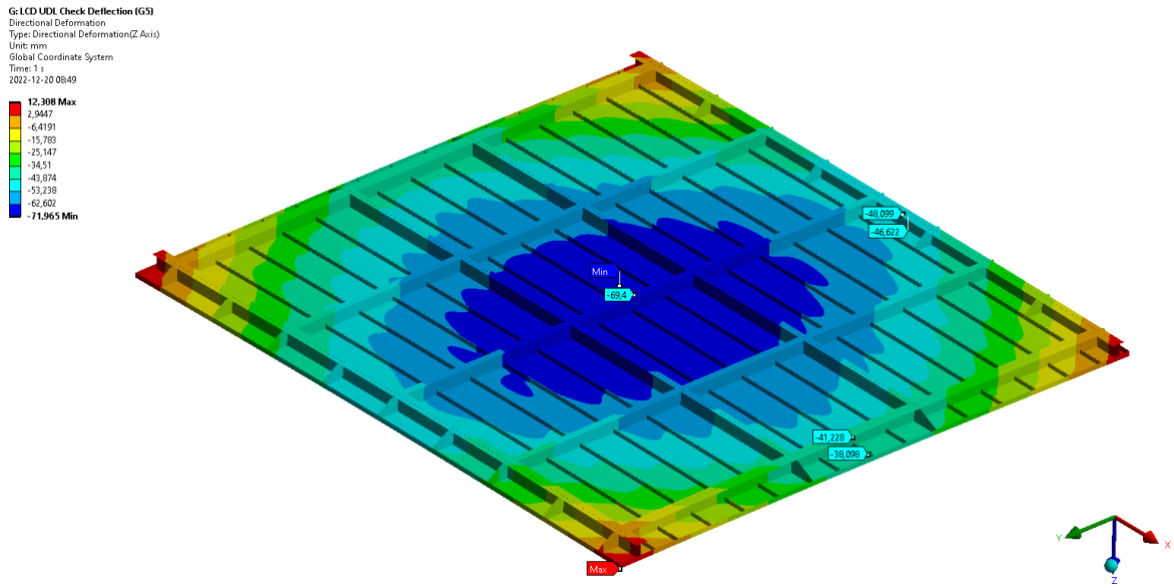

Tabular Data

	Time [s]	Minimum [mm]	Maximum [mm]	Average [mm]
1	1,	-71,965	12,308	-44,778

Figure 4-6. Deflection plot of the new design of Strenx 700 (HT69)

It is noteworthy that here the stress distribution in the original panel is well optimized in terms of stresses in bottom flanges, see Figure 4-3, where the outer main girders have the highest stresses (see Figure 4-3 and Max annotation). It is found that the stress distribution in the STRENX 700 (HT69) panel is not well optimized in terms of stress

level, see Figure 5-4. Since the stresses in the bottom flanges are well below the yield limit of 700 MPa, approximately 350-450 MPa, meaning that the material's capacity is not fully utilized in the existing design.

The use of STRENX 700 (HT69) also results in a substantial increase in panel deflection1. This increase is attributed to the reduced section modulus, a consequence of the thinner plate thickness of STRENX 700 (HT69) being just two-thirds of the original design's thickness. This consequence is something that needs to be addressed since as mentioned previously, increasing the allowable deflection of the panel will cause a higher vessel, meaning that you need to add more material somewhere else instead of the panel.

Deflection is the limiting parameter for the conventional car deck panel. Deflection criteria are a strict parameter, agreed upon with the hull designer. Conventional car deck panels reach the deflection limit before utilizing the materials yield limit of 700 (HT69) MPa. Perhaps a material with a yield limit of 500 MPa could be enough for a conventional design. The possibility of opening up a discussion of the allowable deflections and loads with owners could be interesting if the main goal is to reduce the total weight of the vessel, together with defining the loads clearly, perhaps removing the UDL load case and focusing on the axle load which is a more realistic load for most cases.

4.2 Buckling analysis

Buckling is crucial for car-decks and must be paid special attention. In this project, the buckling analyses of the car-deck are conducted by RISE using Altair OptiStruct, a proven, modern structural solver. Altair OptiStruct has been widely accepted in the automotive industry and has great potential to be applied to thin-wall structures such as car-decks of RoPax vessels. Figure 4-7 shows the FE model of the car-deck in Altair OptiStruct.

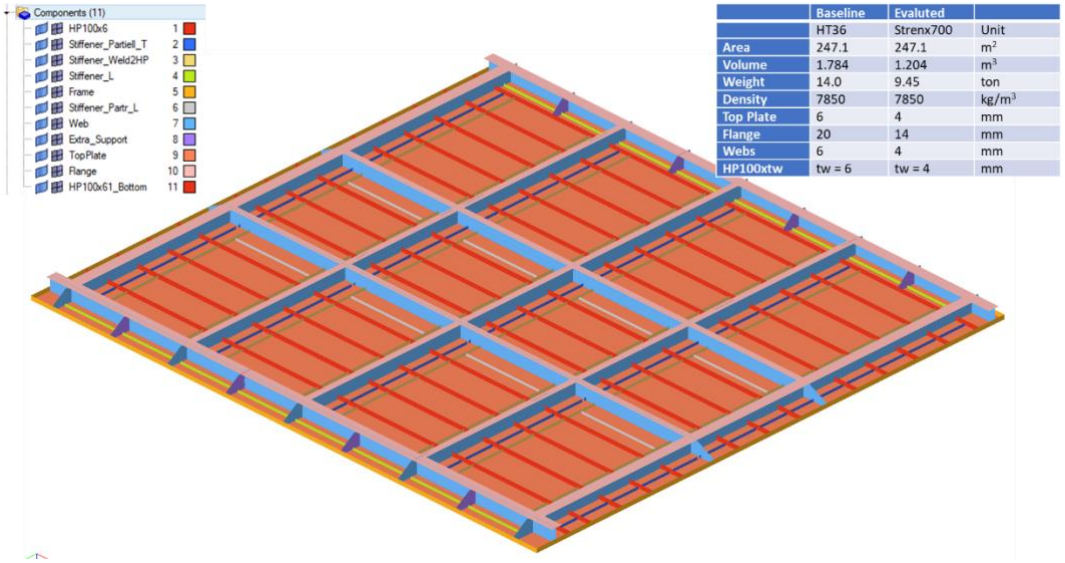

Figure 4-7: CAE setup with the essential information

This section presents an overview of the Altair OptiStruct solution technique for linear buckling analysis. To solve the linear buckling problem in FEA, first apply a loading reference to the structure. A linear static analysis is then performed to determine the stresses required to generate the geometric stiffness matrix at a pre-defined loading level. The buckling loads are then determined by solving an eigenvalue problem.

The solution to the eigenvalue problem usually gives a few eigenvalues. The eigenvalue problem is solved using the Lanczos matrix technique. Buckling analysis often calculates only a fraction of the lowest eigenvalues. The buckling load is represented by the lowest eigenvalue, which is then multiplied by the reference load level to get the critical buckling load.

Three different types of CAE studies are performed on each material category based on the boundary conditions and reference load: non-linear static, linear buckling, and linear static analyses.

4.2.1 Buckling analysis of the Baseline material (HT36)

The car-deck panel is loaded with a Uniformly Distributed Load (UDL) of 300 kg/m2 and a seagoing acceleration of 1.97 x gravity. This load case is taken from a real project and is typically the dimensioning case. The boundary condition is defined as shown in Figure 4-8 where a 3-point constrain method is applied, which is a proper constraint to eliminate all rigid body rotation and translation modes.

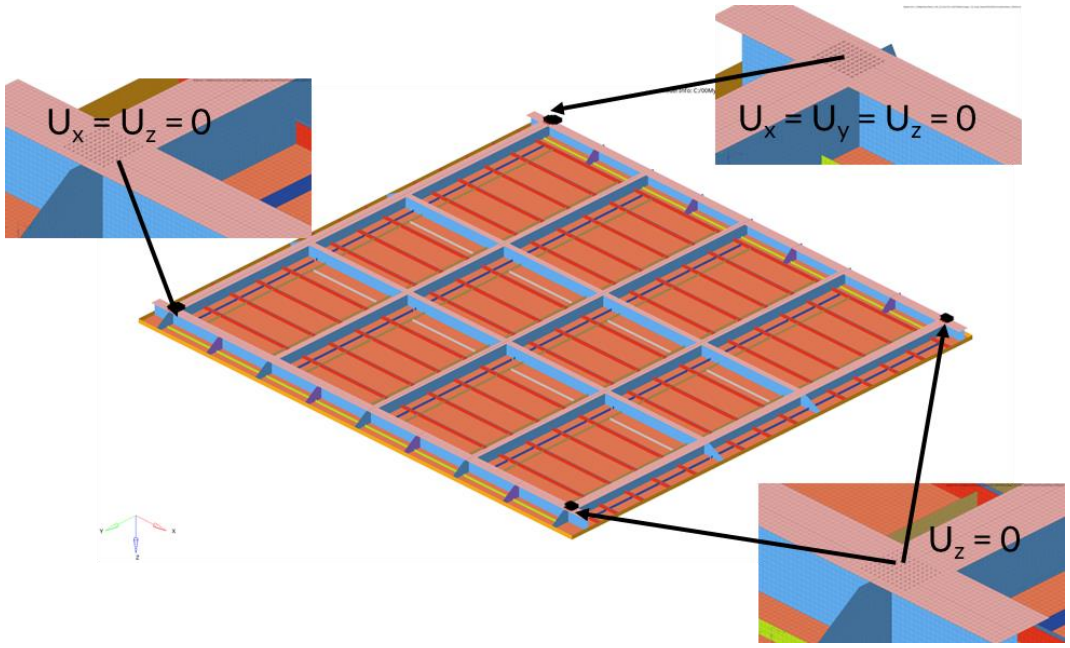

Figure 4-8: Applied boundary condition

Figure 4-9 illustrates the achieved result from the linear FE analysis. The displacement in the middle of the deck is 70mm. However, the results of von Mises stress should be taken with caution since four hotspot locations have been detected between the webs and top plate at four boundary corners, which result in quite high stress concentrations. When the results of these locations are removed, one realizes that the highest amount of stress is roughly 170 MPa (see the red arrow in the image), which is close to 50% of the material yield strength and 30% of the material tensile strength.

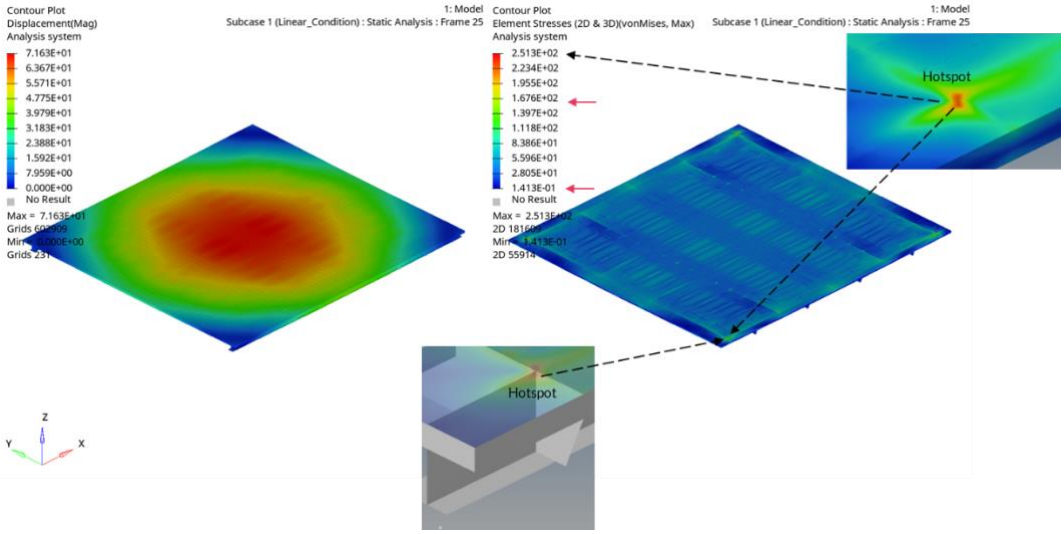

Figure 4-9: Baseline material: Deformation [mm] & Stress distributions [MPa]

The non-linear analysis is used to determine if there is a significant divergence between the numerical results and whether we can expect some non-linear behavior in the structure.

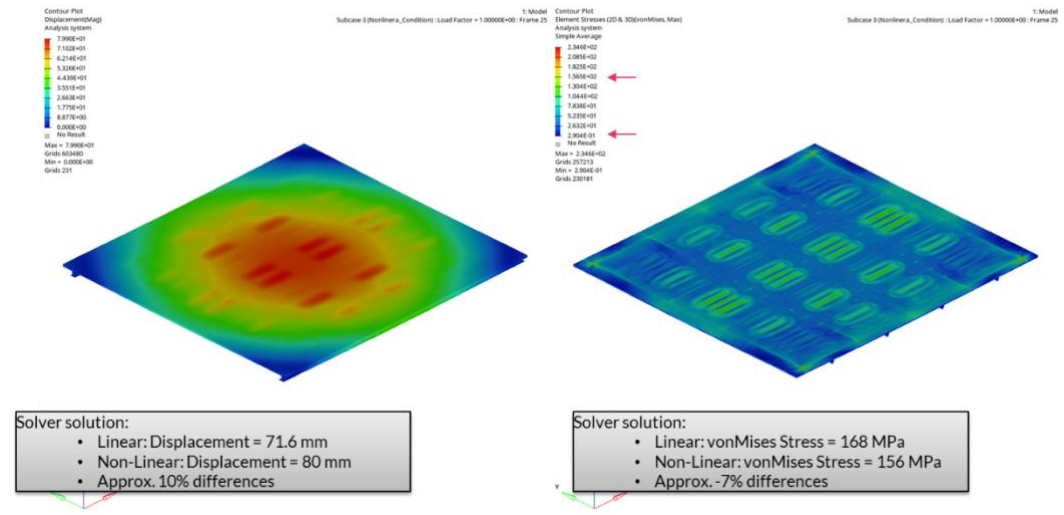

Figure 4-10: Numerical results and comparison between linear and non-linear solutions

In this scenario, the material remains within its elastic limit (the highest von Mises stress is less than 50% of yield strength), and the deformations are minor about the size of the product (70mm vs. 12.8m or 11.8m).

Furthermore, there is no complication in the contact interaction of various components. Figure 4-10 displays the numerical results, using a non-linear solution. The overall deformation and stress distributions differ slightly, but the local deformations between stiffeners may be distinguished.

Nevertheless, the von Mises stress is around 160 MPa, and the displacement in the center of the deck is 80 mm. Since the current case study does not include the impacts of the welding process or initial imperfections on product performance, the linear analysis may be viewed as the worst-case scenario. Future research must take those two last elements into account.

Figure 4-11: displays the results of the buckling analysis for mode 1. As noted in Section 2 (see "the buckling failure modes and four categories"), when stiffeners are strong enough to avoid overall buckling, see Figure 4-11: (right). In local modes, the top panel buckles, as seen in Figure 4-11: (left). These buckling patterns relate to how panels or stiffeners buckle individually. They can also occur concurrently and interact with one another. Figure 4-12 shows the results for the first three buckling modes.

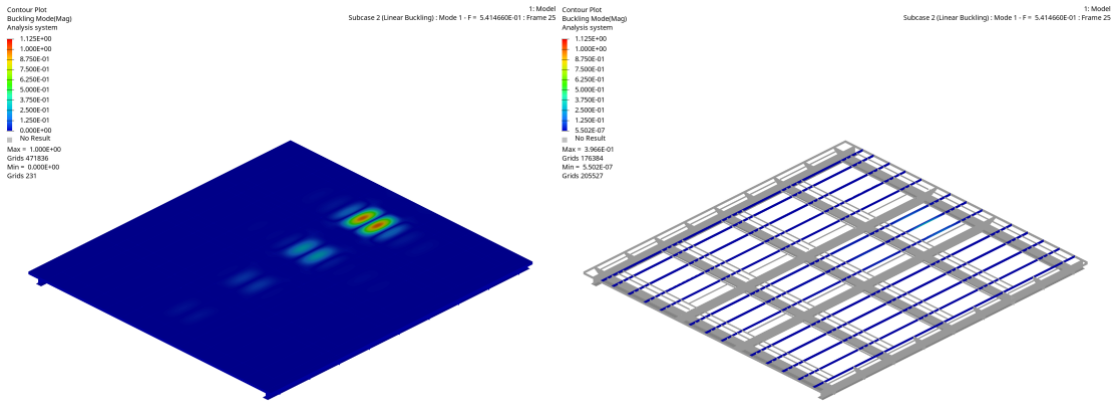

Figure 4-11: Buckling mode1. Left: Plate panel buckling, Right: Stiffener condition

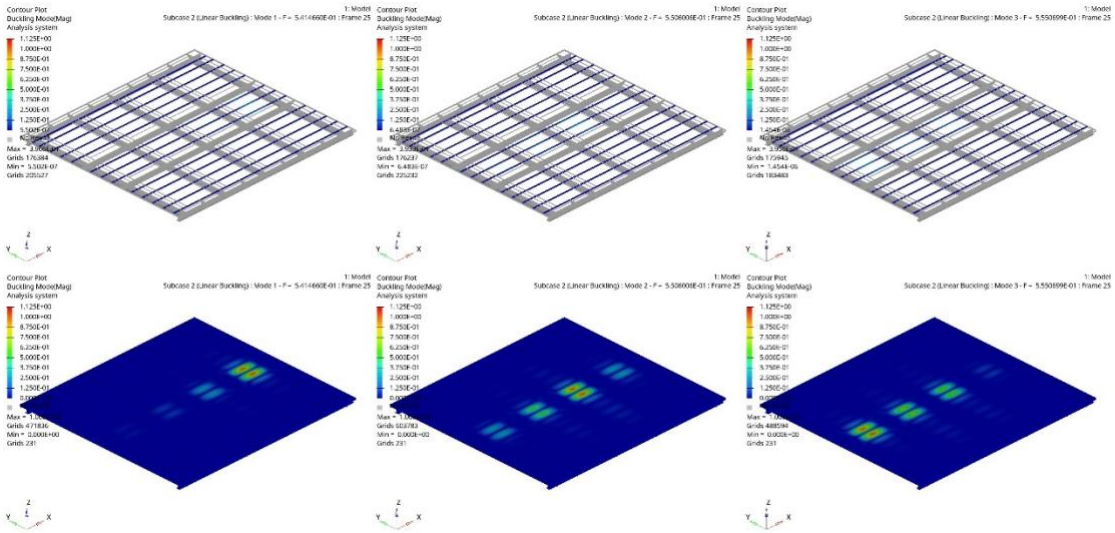

Figure 4-12: Numerical results from Buckling analysis

4.2.2 Buckling analysis of the evaluated material Strenx 700 (HT69)

A similar buckling analysis was carried out for the other material, Strenx 700 (HT69), with modification to geometrical parameters and the identical load condition, with the goal of saving 30% of the total module weight.

Numerical results for a linear structural analysis show (see Figure 4-13) that the total deformation increases by 34% from 71.6 mm to 109 mm in comparison with the baseline material, HT36.

As shown in the figure, the local deformations occur in the center of the panel between stiffeners, which may be related to the thickness of the plate panel. The global von Mises stress increases by only 16%.

The estimated von Mises stress value for Strenx700 (HT69) material is less than 30% of the material's yield strength (approx. 700 MPa) and 20% of the material's tensile strength (approx. 930 MPa).

This might imply that the expected composition of dimensions is a good starting point for continuing the design of the concept with weight reductions. It is vital to note that defects caused by the welding procedure, as well as other faults in the material and process, are not taken into consideration in these simulation models.

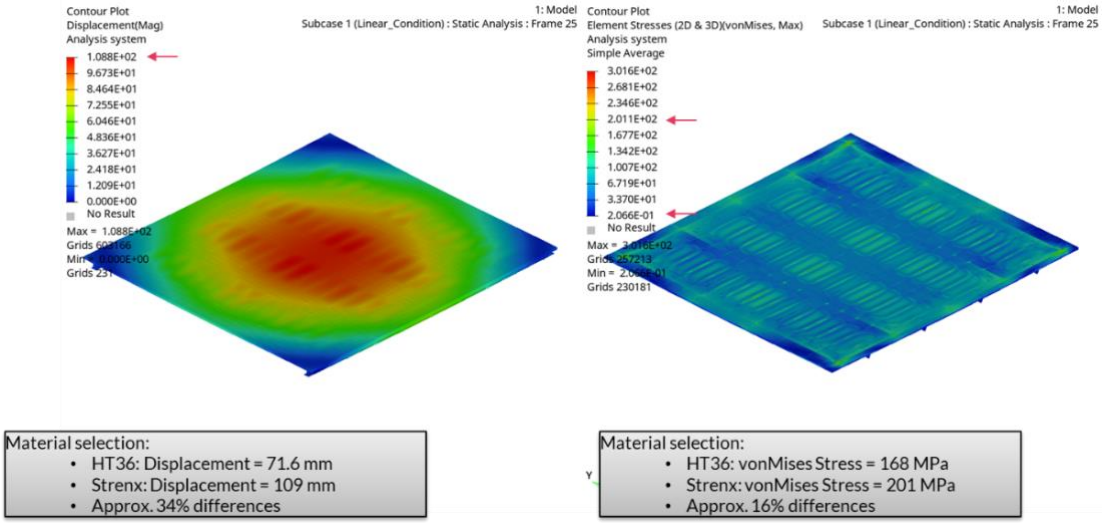

Figure 4-13: Evaluted material Strenx700 (HT69): Deformation [mm] & Stress distributions [MPa] and comparison with baseline material

Figure 4-14 shows the results of the buckling analysis for modes 1–3. The numerical findings are represented by the lowest eigenvalue, which is then multiplied by the reference load level to get the critical buckling load; these values are lower than the estimated values for baseline material.

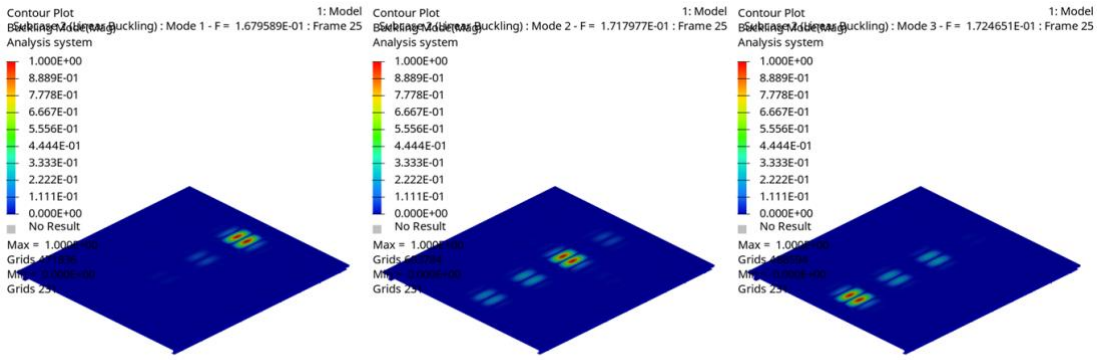

Figure 4-14: Numerical results from Buckling analysis for the first three modes

Note that the critical buckling load for a plate is determined by its width-thickness ratio and support circumstances. Plates' post-buckling behavior, however, is stable, and plates will continue to handle loads greater than their elastic critical loads. This post-buckling range is considerable for plates with high width-thickness ratios (slender plates).

4.2.3 Further parameter study concerning the girder (web) configuration

In the present case, reducing the thickness of the plate panel without modifying the size of other structural components for the deck may be inadequate. Because for materials with the same E-modulus, the critical buckling stress is proportional to plate thickness.

Consider the entire deck as a load-bearing structure. One method is to change the size of support functions like girders and modify the web height and thickness to reduce global deformations. To demonstrate the girder "size" influence on global deformations, the web's dimensions were adjusted with different heights and thicknesses as design parameters and compared to the reference model. The analysis includes four examples, as stated in Table 4-2.

Table 4-2: Web dimensions for each case

Case	Web	
	height [mm]	thickness[mm]
W00t4	327	4
W20t4	347	4
W40t4	367	4
W20t5.5	347	5.5

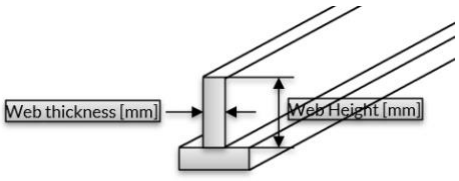

The computational simulations clearly indicate that varying the web thickness (W20t5.5; see Figure 4-15 and Figure 4-16) has a limited effect on global deformations and has a negative impact on weight savings.

Label	Reference value [mm]	Modification [mm]	Web Height [mm]	Web thickness [mm]	Frame Deflection [mm]	vonMises Stress [MPa]	Web Weight [ton]
W00t4	327	00	327	4	104,8	201,4	1,117
W20t4	327	20	347	4	92,83	171,6	1,184
W40t4	327	40	367	4	84,07	146,9	1,251
W20t5,5	327	20	347	5,5	85,88	207,6	1,627

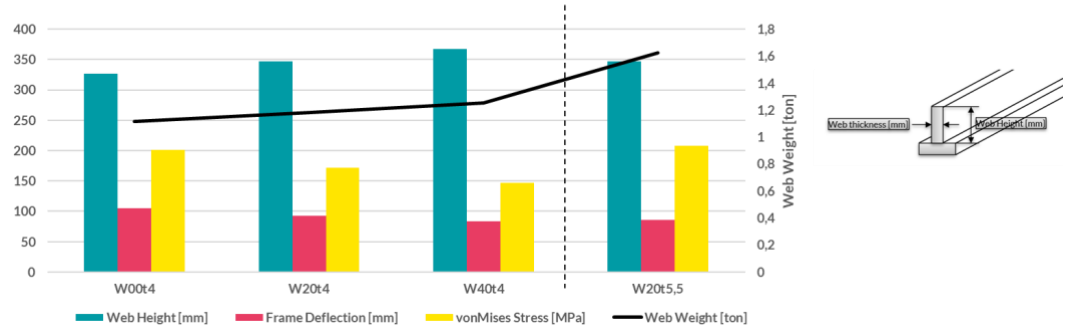

Figure 4-15: Numerical results based on pre-defined cases

Figure 4-16 depicts the data obtained in the form of a parallel diagram with normalized values, demonstrating the web size effect in connection to frame deflection and global stress level.

Label	Reference value []	Modification [-]	Web Height [-]	Web thickness [-]	Frame Deflection [-]	vonMises Stress [-]	Web Weight [-]
W00t4	-	0,00	0,00	0,00	1,00	0,90	0,00
W20t4	-	0,50	0,50	0,00	0,42	0,41	0,13
W40t4	-	1,00	1,00	0,00	0,00	0,00	0,26
W20t5,5	-	0,50	0,50	1,00	0,09	1,00	1,00

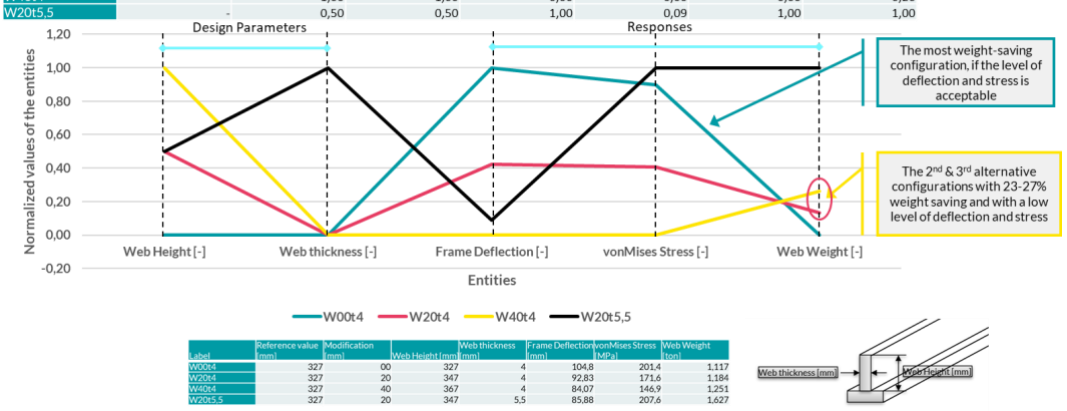

Figure 4-16: Analysis numerical results of the case study using a parallel diagram with normalized values

Nevertheless, as illustrated in Figure 4-17, increasing the web's height by 5-10% may decrease global deformation by 12-24% when compared to the reference case. The adjustments to the web height cause the deck's global deformation level to decrease, consequently resulting in a reduction of stress levels in a loaded condition, see Figure 4-18.

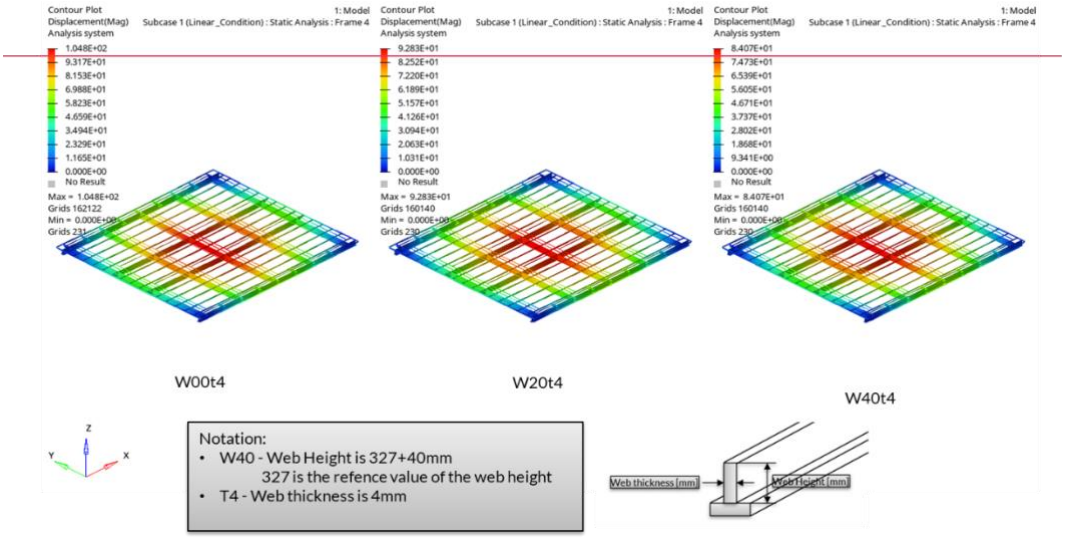

Figure 4-17 FEA results from case study: Displacement distributions [mm]

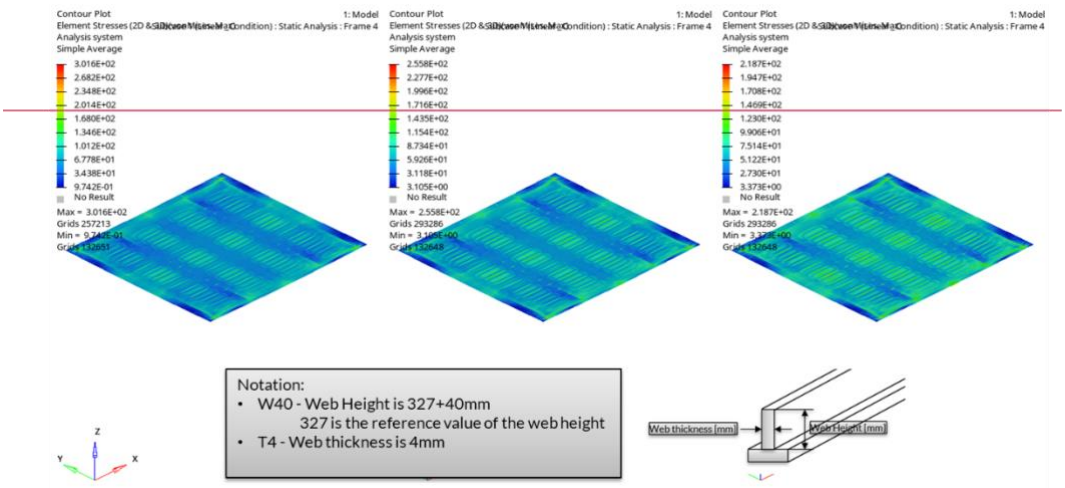

Figure 4-18: FEA results from case study: Stress distributions [MPa]

Note that these concepts have long been used in sandwich theory and construction. The sandwich plate is frequently likened to the I-beam, with the facesheets representing the flanges and the core representing the beam's web.

4.2.4 Control local deflection by introducing embossing

Furthermore, to increase the plate's stiffness and rigidity, local embossing may be necessary to control the local deformations that occur between stiffeners. Figure 4-19 depicts an alternate structural design that uses local reinforcing components instead of stiffeners. It is feasible to reduce the thickness of the specified component (e.g., deck or panel) by about 30% while maintaining product flexural stiffness. This is possible by utilizing the existing stamping capacity with today's technology.

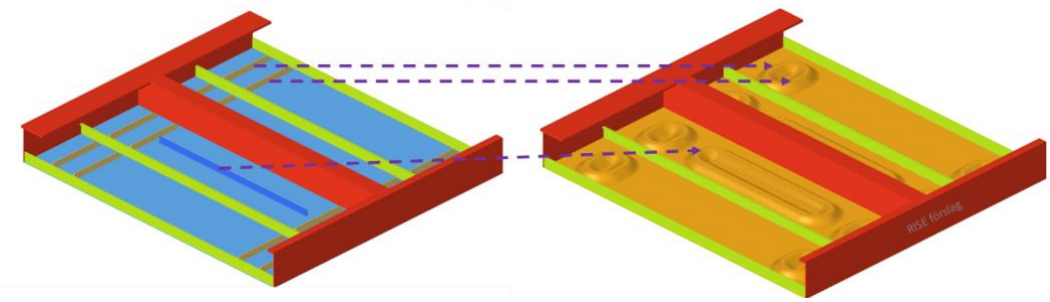

Figure 4-19: A partial section of deck with stiffeners and girder. Left: the standard setup. Right: Plate panel with locally formed region

This is also a frequent technique in the automotive sector, which involves local rigidity.

5 Stern-ramp strength check

In this study, we also carried out a strength check for a stern-ramp of a RoPax vessel, which is illustrated in Figure 5-1. The stern-ramp was designed by MacGregor. The stern-ramp has a dimension of L x B = 9.1 m x 9.3m. The load cases of the stern-ramp are listed as follows:

- Vehicle: MAFI 60t axle + RT 35t boogie
- External sea pressure
- Damage water pressure
- Twisting in port due to heel
- Internal accidental load (Redundancy) IACS
- Maneuvering

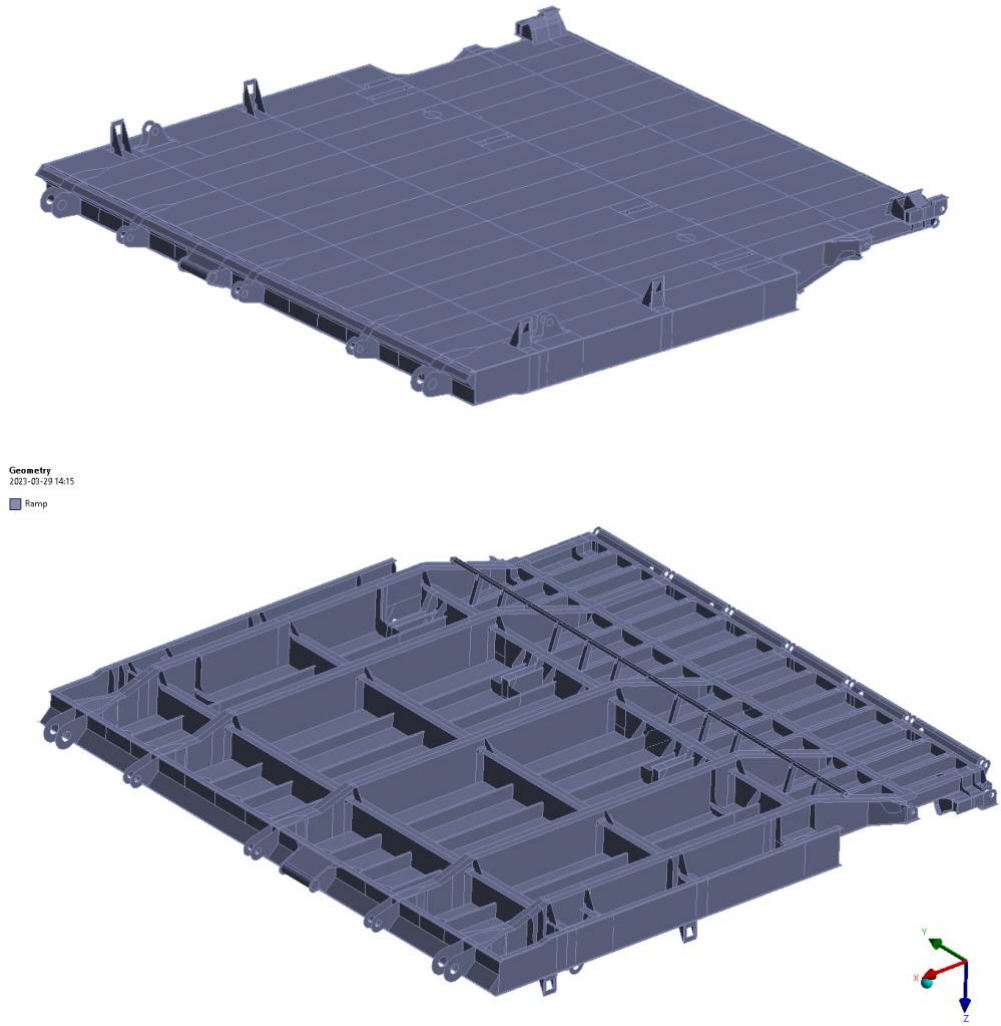

Figure 5-1. Stern-ramp of a RoPax vessel

Similarly to the car-deck panel, MacGregor compared the design of the evaluated material with that of the baseline material. The dimensions are kept for the new design using Strenx700 (HT69), but the steel thickness is cut off by ⅓, following SSAB's recommendation. The material thickness of the stern-ramp of the original design and the new design are presented in Table 5-1. The shell thickness for the original design of the stern-ramp is also illustrated in Figure 5-2.

Table 5-1. Material thickness comparison

HT36	**Strenx 700 (HT69)**
Top plate: 12 mm	Top plate: 8 mm
Flanges: 20 mm	Flanges: 13.3 mm
Webs: 8 mm	Webs: 5.3 mm

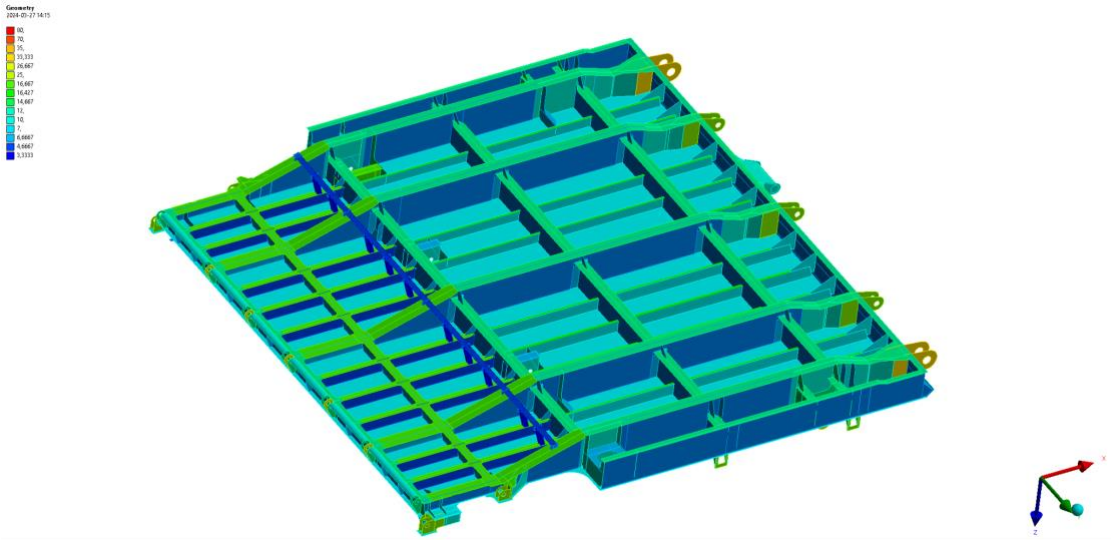

Figure 5-2. Shell thickness for the original design

Similarly to the car-deck, we checked both the stress and deflection of the new design of the higher steel strength. Figure 5-3 and Figure 5-4 show the stress and deflection of the new design of the stern-ramp, respectively. It is observed that the maximum stress of 366 MPa is well below the yield strength of the Strenx700 (HT69). When it comes to the deflection, the criterion from class: L/200 = 9000/200 = 45mm. The maximum deflection of the new design turns out to be 39.6, which is below the limit but the margin is much smaller than the stress. This implies that there is a potential for further thickness reductions, but deflection will become the limiting factor in comparison with the stress.

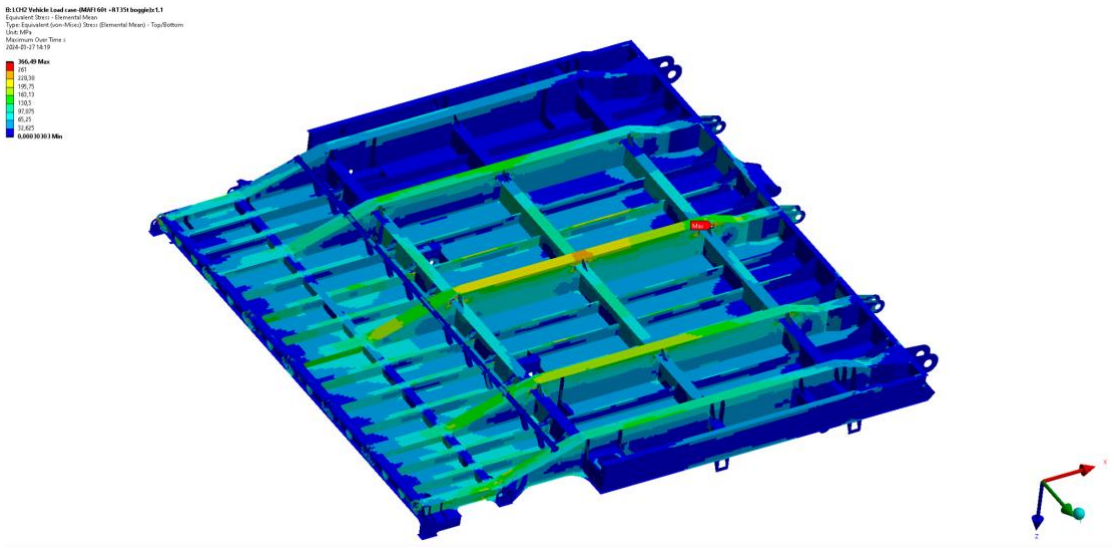

Figure 5-3. Stress plot of the new design of the stern-ramp

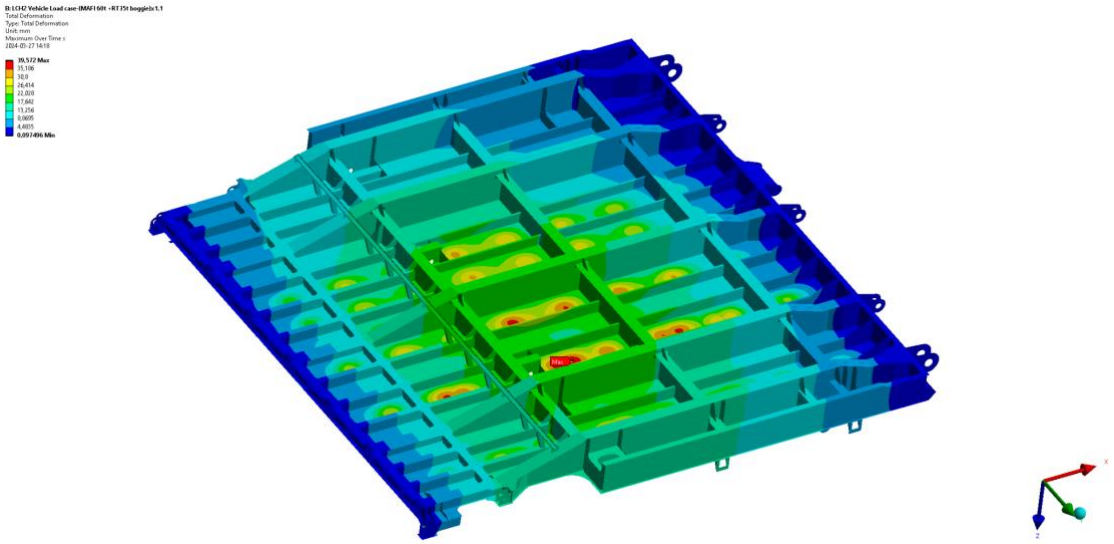

Figure 5-4. Deflection plot of the new design of the stern-ramp.

It must be pointed out that we have not checked the buckling strength for the stern-ramp with higher strength steel induced, which is expected to be one subject of future work.

In summary, a basic comparison similar to the car deck panel has been carried out for a stern-ramp, where a stern-ramp typically has a higher building height and shorter free span (can be different from project to project).

The deflection is therefore not a big problem. It also seems that there is a potential for further thickness reductions of the conventional stern ramp, but more in-depth calculations are needed to verify this.

6 Concluding remarks

In this project, the authors investigated the potential of re-designing ship structures and sub-structures using extra high-strength steels. We propose a practical engineering approach for structural design and optimization of typical ship structure members of stiffened panels using extra high-strength steels with the purpose of weight reduction. The proposed methodology is deemed particularly beneficial for RoPax and RoRo ships, which are represented by large deck areas.

We make use of the methodology of finite element analysis (FEA). Results of buckling analyses from the proposed method are compared with those from the common-accepted PULS, which is a semi-analytical computerized buckling code recognized by DNV and IACS for strength assessment of stiffened thin plate elements as used in ship and offshore structures. The FEA results are found to be agreeable with the PULS results. With the proposed FEA tool, we managed to carry out the following activities:

- Optimization and re-design the representative deck structures with respect to weight with both the buckling capacity and the deflection limit as constraints, and making the increased tensile strength of the new steel material
- Fatigue life comparison between the original design using the baseline steel and the re-design using the extra high strength steel.
- Evaluation of the effect of non-linear buckling behaviors with initial imperfection. The outcome indicates the proposed methodology is a suitable tool for structural re-design and optimization when introducing extra high-strength steels.

In addition, in this work, we selected a Stena RoPax and carried out strength analyses of the car-deck and the stern-ramp. For the car-deck, linear buckling and non-linear analyses were conducted and compared. For the stern-ramp, we focused on the strength check of the limits of the deflection that is specified by the class rules. These analyses again highlighted the great weight-reduction potential of introducing extra high-strength steels in RoPax vessels.

7 References

[1] European Council - EU's target of reducing net greenhouse gas emissions by at least 55% by 2030. https://www.consilium.europa.eu/en/policies/green-deal/fit-for-55/ (Accessed 2024-04-02) (2023).

[2] Llop Sayson, J. P. (2019). Numerical Simulation Assessment of a Ship Dynamic Behavior Against a SSPA Model Test Chalmers university of technology].

[3] 2023 IMO strategy on reduction of GHG emissions from ships, (2023).

[4] Willstrand, O., Ramachandra, V., Evegren, F., Hägg, M., Ramne, B., Li, Z., Thies, F., Ringsberg, J., & Lluis, E. J. (2022). Lätta elfartyg–Electric Light: Lightweight and electrically propelled Ro-Pax ships.

[5] HT36 is a high-tensile steel known for its strength and durability. It's commonly used in structural applications, especially in shipbuilding and construction. Key characteristics include high yield strength, good weldability, Excellent toughness, and use in ship hulls, bridges, and other large structures.

[6] Ni, Xiaoyu & Prusty, Gangadhara & Hellier, Alan. (2016). Buckling and post-buckling of isotropic and composite stiffened panels: A review on optimisation (2000-2015). Transactions of the Royal Institution of Naval Architects Part A: International Journal of Maritime Engineering. 158. A-251 . 10.3940/rina.ijme.2016.a3.388.

[7] Nauticus hull user manual - PULS. In Det Norske Veritas, Høvik, Norway.

[8] The PULS buckling code is available as integrated in Nauticus Hull and Sesam's GeniE, as well as standalone version and as spreadsheet, see https://www.dnv.com/software/faq/which-tools-can-I-use-for-buckling-check-of-a-structural-element-of-a-vessel/

[9] Class Guideline DNV-CG-0128, Buckling. In: Det Norske Veritas, Høvik, Norway.

[10] Mode Snapping is a phenomenon observed in nonlinear systems, particularly those with multiple stable equilibrium points. It occurs when a system suddenly transitions from one stable equilibrium state to another, often in response to a small change in a parameter or external forcing.

[11] DNV. Rules for Classification: Ships. Part 3

[12] D. Radaj, Review of fatigue strength assessment of nonwelded and welded structures based on local parameters, International Journal of Fatigue, Volume 18, Issue 3, 1996, Pages 153-170, ISSN 0142-1123, https://doi.org/10.1016/0142-1123(95)00117-4.

[13] Class Guideline DNV-CG-0129, Fatigue assessment of ship structures. In: Det Norske Veritas, Høvik, Norway

Lighthouse gathers leading maritime stakeholders through a Triple-Helix collaboration comprising industry, society, academies and institutes to promote research, development and innovation within the maritime sector with the following vision:

Lighthouse – for a competitive, sustainable and safe maritime sector with a good working environment

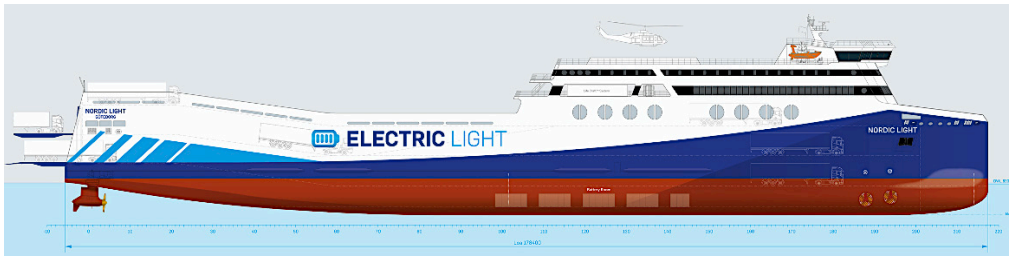

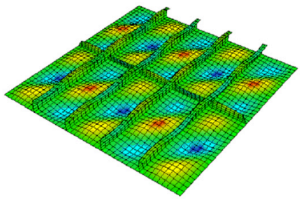

LIGHTHOUSE PARTNERS

CHALMERS · KTH VETENSKAP OCH KONST · Linnéuniversitetet · GÖTEBORGS UNIVERSITET · VÄSTRA GÖTALANDSREGIONEN · SJÖFARTSVERKET · Stiftelsen Sveriges Sjömanshus · SVENSK SJÖFART

LIGHTHOUSE ASSOCIATE MEMBERS

BUREAU VERITAS · ivl · RI.SE · SSPA Your Maritime Solution Partner · vti · DNV